

ON SN 2003fg: THE PROBABLE SUPER-CHANDRASEKHAR-MASS SN Ia

David J. Jeffery¹, David Branch¹, & E. Baron¹

ABSTRACT

Howell et al. have reported the discovery of SN Ia SN 2003fg (SNLS-03D3bb) and conclude that SN 2003fg is very likely a super-Chandrasekhar-mass SN Ia perhaps with a mass $\sim 2 M_{\odot}$. Their work is the first strong evidence that has been presented for a super-Chandrasekhar SN Ia. We have performed an analysis of the SN 2003fg data using the Yoon & Langer binding energy formula for a rotating super-Chandrasekhar-mass white dwarf (also used by Howell et al.) included in a simple model of SNe Ia (which we call the SSC model for Simple Super-Chandrasekhar model for SNe Ia) which assumes spherically symmetric ejecta and relies on the approximations of an exponential density profile for SN Ia ejecta and of a sharp boundary of the SN Ia iron-peak-element core. Our results support the conclusion of Howell et al.: SN 2003fg is very probably super-Chandrasekhar and probably has mass $\sim 2 M_{\odot}$.

Subject headings: supernovae: general — supernovae: SN 2003fg (SNLS-03D3bb)

1. INTRODUCTION

Recently, Howell et al. (2006, hereafter H2006), as part of the Supernova Legacy Survey (SNLS), have reported the discovery of SN Ia SN 2003fg (supernova SNLS-03D3bb in the SNLS naming scheme). SN 2003fg is a remote supernova at $z = 0.2440 \pm 0.0003$ and using concordance cosmology ($H_0 = 70 \text{ km s}^{-1} \text{ Mpc}^{-1}$, $\Omega_M = 0.3$, flat universe) is found to be about 2.2 times brighter in absolute V magnitude than the median brightness of SNe Ia: it is intrinsically the brightest SN Ia known with any confidence. SN 2003fg's lightcurves in shape are not out of the range of normal SN Ia behavior. Thus, SN 2003fg strongly violates the lightcurve width-luminosity relationship (Phillips 1993; Phillips et al. 1999) which is so useful in cosmology.

¹Homer L. Dodge Department of Physics & Astronomy, University of Oklahoma, 440 W. Brooks St., Norman, Oklahoma 73019, U.S.A.

The one spectrum published by H2006, which comes from 2 days after B maximum (light) (which H2006 assume to also be bolometric maximum light), looks typical of near- B -maximum SN Ia spectra as H2006’s Figure 3 shows by a comparison to the very normal SN Ia SN 1994D (a core normal SN Ia in the terminology of Branch et al. (2006)). The spectrum line features, however, are distinctly narrow. The narrowness suggests somewhat low ejecta velocities for the region of line formation in comparison to normal SNe Ia at the same phase. (The width of the lines is determined by the Doppler shift of line opacity in the expanding ejecta.) The line velocity of SN 2003fg’s Si II $\lambda 6355$ line (e.g., Wiese et al. 1969, p. 79) (the line which is the most characteristic line of SNe Ia) in the spectrum is $8000 \pm 500 \text{ km s}^{-1}$. (Line velocity is the Doppler shift velocity corresponding to the wavelength shift of a P Cygni line absorption trough minimum from the line center wavelength. As supernovae evolve the line velocities generally decrease because the ejecta density is falling and the region of sufficient opacity to form lines recedes into the ejecta in mass fraction and velocity.) Core normal SNe Ia have photospheric velocities of $\sim 11000 \text{ km s}^{-1}$ at 2 days after B maximum (Branch et al. 2005, 2006). Since the photospheric velocity is a lower limit on line velocities with normal line formation, SN 2003fg’s photospheric velocity was unusually low for its phase and probably $\sim 8000 \text{ km s}^{-1}$ which is, in fact, the photospheric velocity given by H2006 in their supplementary information²

Note that supernovae after very early times have all mass elements approximately in uniform motion, and thus all ejecta structures just scale up linearly with time since explosion t . This kind of expansion is called homologous expansion. In homologous expansion, the radii r of all mass elements obey

$$r \approx vt , \tag{1}$$

where v is the mass element velocity and initial radial position in the progenitor is considered negligible. Because of equation (1), velocity becomes a good comoving frame coordinate for describing supernova ejecta and we conventionally use it as such. Also in homologous expansion, all mass element densities scale as t^{-3} .

The photospheric velocity is the characteristic velocity of the layer of continuum emission. In the case of SNe Ia, the continuum is not a pure blackbody continuum. Because of falling density and thus opacity, the photosphere, like the line formation region, recedes into the ejecta in velocity coordinate with passing time. As the photosphere recedes, the P Cygni lines gradually transform to emission lines. Eventually, the photosphere vanishes altogether. The photospheric phase of a supernova is when the photosphere is still important to the radiative transfer. After the photospheric phase is the nebular phase. The transition

²See URL <http://www.nature.com/nature/journal/v443/n7109/supinfo/nature05103.html> .

between the two phases is, of course, gradual.

One point to emphasize is that the SN 2003fg spectrum in the optical was dominated by intermediate-mass element (IME) lines and not iron-peak element (IPE) lines. (We consider carbon through calcium as IMEs and scandium through nickel as IPEs.) Optical spectrum dominance in the early post- B -maximum phase by IME lines (principally those of Si II, S II, and Ca II) is true for all SNe Ia, not just normal ones. This shows that the spectrum formation is not primarily in what we call the IPE core of the ejecta, but at higher velocities. Most SNe Ia show IME-line dominance in the optical spectra in the pre- B -maximum and B -maximum phases as well.

The IPE core is the interior region of many SN Ia explosion models that is almost entirely IPEs. At time zero after the explosion the IPE core is in fact mainly radioactive ^{56}Ni . The IPE core is a standard feature of explosion models that result from the standard SN Ia model. In the standard SN Ia model, the progenitor is a carbon-oxygen white dwarf (a CO WD with about equal amounts of C and O) that is very close to the physical Chandrasekhar mass ($1.38 M_{\odot}$ for CO WDs with equal amounts of C and O: see Appendix A) with typical central densities of order $3 \times 10^9 \text{ g cm}^3$ and typical central temperatures of order $2.5 \times 10^8 \text{ K}$ (e.g., Woosley & Weaver 1994, p. 108). With such densities and temperatures unstable carbon burning will initiate an explosion that totally disrupts the WD and creates a SN Ia. The WD is driven to the explosive state by mass accretion from a binary companion. The companion is probably a post-main-sequence star of some kind although the possibility exists that it may be another WD that is merging with the first WD at least in some cases (e.g., Piersanti et al. 2003): the first case is the single-degenerate scenario and the second, the double-degenerate scenario. The double-degenerate scenario has been considered as a channel to super-Chandrasekhar SNe Ia (i.e., SNe Ia with mass greater than the Chandrasekhar mass). The accreted second WD in the double-degenerate case could form an extended envelope around the first WD (e.g., Webbink 1984). In this picture, there is no real super-Chandrasekhar WD. At present, the double-degenerate scenario is moot. Some contend that mergers of two WDs cannot lead to SNe Ia, but rather to collapse to a neutron star eventually, (e.g., Saio & Nomoto 2004) and others that they can (e.g., Piersanti et al. 2003). We will only consider the single-degenerate scenario in this paper since at present it seems most favored and since it offers a plausible channel to super-Chandrasekhar SNe Ia (see below).

In the single-degenerate scenario, if a WD gets sufficiently close to the Chandrasekhar mass and is non-rotating, it should collapse to a neutron star. (Electron capture on nuclei brings about collapse before the physical Chandrasekhar mass is reached: see Appendix A.) SNe Ia happen because in some cases unstable nuclear burning explodes the WDs before

the point of collapse is reached. In the explosion, nuclear burning turns the inner part of the ejecta into nearly pure IPEs with the dominant isotope being radioactive ^{56}Ni : this inner part is the IPE core. Outside of the IPE core, IPEs are trace elements. Immediately outside of the IPE core, the composition in most explosion models is dominated by explosion-synthesized silicon and sulfur. Above that is a layer dominated by explosion-synthesized and pre-existing oxygen with probably relatively large abundances of explosion-synthesized silicon and magnesium. There may be an outer layer or region of pre-existing CO that survives the burning in some SNe Ia. Carbon lines have been tentatively identified in a few SNe Ia (e.g., Jeffery et al. 1992; Fisher et al. 1999; Branch et al. 2003).

The existence of a somewhat layered composition for SNe Ia, including in particular an IPE core, seems almost certain. Such compositions are the result of partially successful near-Chandrasekhar-mass, one-dimensional, hydrodynamic explosion models (e.g., Nomoto et al. 1984; Thielemann et al. 1986; Woosley 1991; Woosley & Weaver 1994; Khokhlov et al. 1993; Höflich & Khokhlov 1996; Höflich et al. 1998) and are indispensable in modeling SNe Ia with synthetic spectra. A reference SN Ia explosion model of longstanding exhibiting a layered composition is the one-dimensional deflagration model W7 (Nomoto et al. 1984; Thielemann et al. 1986). In many respects model W7 seems to approximate normal SN Ia behavior to some degree (e.g., Baron et al. 2006)³. Model W7 does, in fact, have an outer layer of unburnt CO (with a trace of Ne) of $0.098 M_{\odot}$ (Thielemann et al. 1986). The unburnt mass fraction is 0.071. One-dimensional Delayed-detonation models, which have also been partially successful SN Ia models, typically have much less unburnt mass. For example, the near-Chandrasekhar-mass delayed-detonation models of Khokhlov et al. (1993) have an unburnt mass fraction of order 0.01 and those of Höflich et al. (1998) have an unburnt mass fraction of order 0.001. Based on this evidence, it is probable that normal SNe Ia have unburnt mass fraction $\lesssim 0.07$.

A vital part of the standard SN Ia model is the synthesis of the radioactive ^{56}Ni in the explosion. The ^{56}Ni is the overwhelmingly dominant source of radiation energy for the observable phase of SNe Ia. The decay chain for ^{56}Ni is $^{56}\text{Ni} \rightarrow ^{56}\text{Co} \rightarrow ^{56}\text{Fe}$ with half-lives of 6.077 ± 0.012 days and 77.27 ± 0.03 days for the first and second decays, respectively (e.g., Firestone & Ekström 2004).

H2006’s analysis of the high luminosity of SN 2003fg led to the conclusion that SN 2003fg had a very high mass of ^{56}Ni and a (total) mass of $\sim 2 M_{\odot}$, and thus that SN 2003fg was super-Chandrasekhar. They posit that the progenitor reached a super-Chandrasekhar

³Plots of model W7’s density profile and composition, and data files that fully specify model W7 are available at <http://www.nhn.ou.edu/~jeffery/astro/sne/spectra/model/w7/w7.html>.

mass before exploding because it had high angular momentum and the centrifugal force gave it extra support against collapse. High angular momentum is possible because the accretion process could substantially increase the initial WD angular momentum. But before SN 2003fg, there has been no strong evidence for super-Chandrasekhar SNe Ia.

In § 2, we discuss the SN 2003fg ^{56}Ni mass and (total) mass and H2006’s analysis. Section 3 discusses the SN Ia IPE-core boundary and IPE-core velocity which are relevant to our analysis of SN 2003fg. Section 4 introduces our SN Ia model (the SSC model) for the analysis of the SN 2003fg ^{56}Ni mass and mass. In § 5, we compare the predictions of the SSC model to observations for a sample of low- z SNe Ia from Benetti et al. (2005) and in § 6, to the observations for SN 2003fg. Conclusions and discussion are given in § 7. Appendix A discusses the meaning and values of the Chandrasekhar mass. Appendix B presents the rotating CO WD binding energy formula of Yoon & Langer (2005, hereafter YL) which H2006 used and which we use in the SSC model and some related results for this binding energy formula. Appendix C shows how to solve the SSC model for SN Ia mass when SN Ia mass is a dependent parameter. Appendix D shows how to solve the SSC model for IPE-core mass when IPE-core mass is a dependent parameter.

2. THE SN 2003fg ^{56}Ni MASS AND TOTAL MASS

If we did not know that SN 2003fg was intrinsically exceptionally luminous, it would seem like an only somewhat peculiar SNe Ia and would attract only modest special attention. But its luminosity and its violation of the lightcurve width-luminosity relationship makes it an exceptionally interesting SN Ia. In order to produce SN 2003fg’s unusual luminosity, H2006 have calculated that it had a mass of explosion-synthesized radioactive ^{56}Ni of $M_{56\text{Ni}} = 1.29 \pm 0.07 M_{\odot}$.

The calculation for $M_{56\text{Ni}}$ made use of the relationship

$$M_{56\text{Ni}} = \frac{L_{\text{bol}}}{\alpha \dot{E}_{56\text{Ni}}(t_{\text{bol}})}, \quad (2)$$

where L_{bol} is the maximum of bolometric luminosity (which is emitted radiation integrated from the ultraviolet to the infrared), $\dot{E}_{56\text{Ni}}(t_{\text{bol}})$ is the instantaneous rate of release of radioactive decay energy per unit mass of ^{56}Ni by ^{56}Ni and its daughter isotope ^{56}Co at the time of maximum bolometric luminosity t_{bol} , and α is a correction factor to account for time delay in the radioactive decay energy being emitted from the ejecta. H2006’s value for $L_{\text{bol}}/\dot{E}_{56\text{Ni}}(t_{\text{bol}})$ is $1.55 M_{\odot}$. From analytic solutions for the early SN Ia lightcurves, Arnett (1979, 1982) found that α should be 1 exactly. In realistic SNe Ia models and in real SNe Ia,

one would expect a multiplicity of interacting effects will cause α to be only of order 1 and that there will be a range of values with the value for any case depending on that case in perhaps a complex way. An early survey of SN Ia lightcurve calculations suggested $\alpha = 1.2 \pm 0.2$ (Branch 1992), where the uncertainty represents the range of values. An extensive set of SN Ia lightcurve calculations (Höflich & Khokhlov 1996) gives α values that extend over the range 0.71–1.46 for models that are at least partially successful in fitting lightcurves of one or more SNe Ia: the SNe Ia included normal SNe Ia and peculiar SNe Ia of various sorts. The full α range (for models including those that are not acceptable for known SNe Ia) is 0.62–1.46 with mean 1.01 and standard deviation 0.20. There are no unambiguous correlations of the α values with $M_{56\text{Ni}}$, rise time to bolometric maximum light, or model category (Höflich & Khokhlov 1996, Table 2, Fig. 7). However, physically there should be a tendency for α to be relatively small if significant ^{56}Ni matter is near the surface which would happen necessarily if the ^{56}Ni mass was a very large fraction of the ejecta mass. This tendency is because some of the radioactive decay gamma-rays can escape the ejecta directly from near the surface, and thus not deposit their energy in the ejecta: such escaping gamma-rays are not included in the conventional bolometric luminosity. There is a hint of the gamma-ray-escape effect in the results of Höflich & Khokhlov (1996), but it is not clear how to identify it among all the other interacting effects. Actually most of the calculated lightcurves of Höflich & Khokhlov (1996) have rise times to bolometric maximum light that are too short for most SNe Ia for which the mean rise time (using B band as a proxy for bolometric luminosity) is ~ 19 days (Conley et al. 2006). Nevertheless, the calculations of Höflich & Khokhlov (1996) are suggestive of the range of α behavior that may hold for SNe Ia and we keep that in mind for our analysis in §§ 5 and 6. We also will keep in mind though that SN 2003fg is a very peculiar and a unique SN Ia, and so its α value is not well constrained by the α values of existing SN Ia models and other known SNe Ia.

Following Branch (1992), H2006 adopted $\alpha = 1.2$ (which we will consider as the fiducial value) for all their calculations of $M_{56\text{Ni}}$, but did not consider any variations of α nor include the uncertainty of α in their uncertainty calculations. In fact, their other uncertainties (in bolometric luminosity L_{bol} and rise time to bolometric maximum light t_{bol}) are negligible in comparison to the uncertainty in α .

Typically, SNe Ia are thought to have of order $0.6 M_{\odot}$ of ^{56}Ni . For the sample of well-observed 26 low- z SNe Ia studied by Benetti et al. (2005) (hereafter the low- z sample), H2006 calculate a $M_{56\text{Ni}}$ range of $\sim 0.04\text{--}0.86 M_{\odot}$ (using $\alpha = 1.2$). Thus, H2006’s value of $M_{56\text{Ni}} = 1.29 \pm 0.07 M_{\odot}$ for SN 2003fg is well outside of the normal $M_{56\text{Ni}}$ range and is the highest ever calculated with reasonable confidence provided we assume SN 2003fg has no extreme variation in α from the fiducial value of 1.2. (We will consider the possible variations in α and their effects on (total) SN Ia mass estimates in §§ 5 and 6.) Note that

the uncertainties of $L_{\text{bol}}/\dot{E}^{56\text{Ni}}(t_{\text{bol}})$ for the low- z sample are in some cases greater than for SN 2003fg because some of these SNe Ia are not well out in the Hubble flow where distances can be determined with higher accuracy. (Uncertain reddening corrections may also be a problem, but reddening corrections were not discussed by H2006.) Thus, the $M_{56\text{Ni}}$ values for the low- z sample are more uncertain than for SN 2003fg.

The possibility of SNe Ia with very high ^{56}Ni mass has been raised in the past. Assuming a long distance for the SN 1991T host galaxy NGC 4527 of 16.4 ± 1.0 Mpc, Fisher et al. (1999) suggest a ^{56}Ni mass of $\gtrsim 1.4 M_{\odot}$ for SN 1991T. However, Cepheid distances to NGC 4527 of 13.0 ± 1.7 Mpc (Gibson & Stetson 2001) and 14.1 ± 0.8 Mpc (Saha et al. 2001) imply a less luminous SN 1991T, and thus a lower ^{56}Ni mass that is in or closer to the normal range. For SN 1991T, H2006 find $M_{56\text{Ni}} = 0.86 M_{\odot}$ using $\alpha = 1.2$: it is not clear what distance they adopted for NGC 4527. Several SNe Ia or possible SNe Ia have very uncertain absolute B maxima (Richardson et al. 2002) that are about as bright or even brighter than that of SN 2003fg. The most outstanding example is possible SN Ia SN 1988O for which the brightest observed absolute B magnitude is ~ -21.3 (using $H_0 = 70 \text{ km s}^{-1} \text{ Mpc}^{-1}$), but probably with great uncertainty (Richardson et al. 2002). This B value is ~ 1.2 magnitudes brighter than SN 2003fg’s absolute B maximum of -20.09 (H2006). The uncertainties are such that there is no confidence at present that any of the possibly very bright SNe Ia are as bright or have ^{56}Ni mass comparable to SN 2003fg.

The high ^{56}Ni mass of SN 2003fg has dramatic implications for SN 2003fg’s (total) mass. As discussed in § 1, in the standard SN Ia model, a SN Ia has only about a physical Chandrasekhar mass $1.38 M_{\odot}$ since that is the standard-SN-Ia-model mass of its WD progenitor. However, accreting, rotating WDs can exceed the Chandrasekhar mass before reaching the density and temperature conditions for explosion. The centrifugal force provides the WD with extra support against gravity. YL believe that WDs of up to $\sim 4 M_{\odot}$ are dynamically possible, but that possible accretion histories may limit them to not much more than $2 M_{\odot}$ (Langer et al. 2000).

Given that the calculated SN 2003fg ^{56}Ni mass is so close to the Chandrasekhar mass, it is difficult on simple grounds to believe that SN 2003fg’s mass is only nearly a Chandrasekhar mass. If SN 2003fg were a near-Chandrasekhar-mass SN Ia and its radiative transfer history not exotic, then its photosphere would be well inside its IPE core near B maximum for density profiles that work well for normal SNe Ia. An IPE core of $1.29 M_{\odot}$ of ^{56}Ni and nothing else (which is implausible) in a near-Chandrasekhar-mass SN 2003fg with a model-W7 density profile would extend to $\sim 15000 \text{ km s}^{-1}$ (Nomoto et al. 1984, Fig. 4). If this were the case, the SN 2003fg 2-days-past- B -maximum spectrum would be dominated by IPE lines and, as discussed in § 1, this is not observed. To keep the 2-days-past- B -maximum

spectrum looking normal, the actual SN 2003fg IPE-core velocities must probably have been kept below $\sim 8000 \text{ km s}^{-1}$ (the SN 2003fg photospheric velocity for 2 days past B maximum: § section-intro) by much more than $0.1 M_{\odot}$ of overlying mass.

A simple scaling argument gives a possible mass for SN 2003fg. Assume that the ratios of ^{56}Ni mass $M_{^{56}\text{Ni}}$ and other elements to mass M are roughly constant for SNe Ia of any mass. Then mass will roughly scale with ^{56}Ni mass. If the average SN Ia has $0.6 M_{\odot}$ of ^{56}Ni and a near-Chandrasekhar mass, then SN 2003fg would have a mass of

$$M \approx \frac{1.29}{0.6/1.4} = 3.0 M_{\odot} . \quad (3)$$

If we now assume that $\sqrt{2E/M}$ is approximately a constant as mass is varied, the ejecta velocities for the various matter elements of SNe Ia will be crudely invariant with mass since velocities for the various matter elements overall scale approximately as $\sqrt{2E/M}$. Thus, a $3 M_{\odot}$ SN 2003fg could have the velocities of line formation near B maximum that were not wildly different from those of normal SNe Ia provided the photospheric velocity evolution was not wildly different from that of normal SNe Ia. The assumptions we made to obtain the estimate of $3 M_{\odot}$ for SN 2003fg are at most only partially valid, and thus the estimate is only suggestive. We verify in Appendix B that $\sqrt{2E/M}$ can be crudely accepted as constant with mass M provided super-Chandrasekhar SNe Ia are approximated by our SSC model (see § 4) up to masses of $3 M_{\odot}$.

Another estimate of the SN 2003fg mass follows from an argument given by H2006 that we modify a bit here. If an average SN Ia has a near-Chandrasekhar mass and $M_{^{56}\text{Ni}} = 0.6 M_{\odot}$, then it has about $0.8 M_{\odot}$ of non- ^{56}Ni matter. If SN 2003fg is to look as spectroscopically normal as it does, then perhaps it should have of order the same amount of non- ^{56}Ni matter. It follows then that the SN 2003fg mass could be $\sim 2.1 M_{\odot}$. This mass estimate is also only suggestive.

H2006 also estimate the SN 2003fg mass from a simple SN Ia model that allows for super-Chandrasekhar mass since it assumes a rotating WD progenitor and that has 4 independent parameters: (total) mass M , mass of explosion-synthesized IPEs $M_{\text{IPE-core}}$, surviving unburnt CO mass fraction f_{CO} , and progenitor WD central density $\rho_{\text{central,WD}}$. H2006 apparently in all cases set $\rho_{\text{central,WD}} = 4 \times 10^9 \text{ g cm}^{-3}$ which can be regarded as of order a typical progenitor WD central density. We use the symbol $M_{\text{IPE-core}}$ for the explosion-synthesized IPE mass since for the SSC model (introduced in § 4), we will make the assumption that all the explosion-synthesized IPEs are in the IPE core and no other matter is in the IPE core. H2006 do not, in fact, make this assumption although it does not change their model much to do so. For the sake of consistent notation, we will use $M_{\text{IPE-core}}$ for the description of H2006’s model. The mass fractions of the ejecta of explosion-synthesized IMEs and

explosion-synthesized IPEs are, respectively, f_{IME} , and f_{IPE} . (Note carbon and oxygen are IMEs, but the unburnt amount of CO is not included in f_{IME} .) These are not independent parameters since

$$f_{\text{IPE}} = \frac{M_{\text{IPE-core}}}{M} \quad \text{and} \quad f_{\text{IME}} = 1 - f_{\text{CO}} - f_{\text{IPE}} . \quad (4)$$

Actually, to obtain model parameter $M_{\text{IPE-core}}$ from $M_{56\text{Ni}}$, one needs a conversion factor

$$g = \frac{M_{56\text{Ni}}}{M_{\text{IPE-core}}} . \quad (5)$$

H2006 adopt $g = 0.7$. The rationale for this value is as follows. The deflagration model W7 gives $g = 0.70$ (Nomoto et al. 1984; Thielemann et al. 1986) (although to find this number accurately one must examine the model W7 data files) and the pure detonation model DET1 (which is not a reasonable model for any SN Ia) gives $g = 0.66$ (Khokhlov et al. 1993). Models W7 and DET1 are rather remote from each other in model space, and so the fact that they yield similar g values near 0.7 suggests that $g = 0.7$ is a good representative fiducial value. Obviously g must be in the range 0 to 1.

From equations (2) and (5), the full formula for $M_{\text{IPE-core}}$ is

$$M_{\text{IPE-core}} = \frac{L_{\text{bol}}}{g\alpha\dot{E}_{56\text{Ni}}(t_{\text{bol}})} . \quad (6)$$

As mentioned above, we believe that the uncertainties in the SN 2003fg L_{bol} and t_{bol} are negligible in comparison to the uncertainty of α for SN 2003fg. The uncertainty in g for SN 2003fg may be smaller than that of α , but it is still not very well constrained. In our analysis in §§ 5 and 6, we will consider how the results change when varying α and g and neglect uncertainties in L_{bol} and t_{bol} .

The kinetic energy of H2006's SN Ia model is the energy released by nuclear burning minus the binding energy of the WD progenitor and is assumed to be given by

$$E = E_{\text{IPE}}M[f_{\text{IPE}} + R(1 - f_{\text{CO}} - f_{\text{IPE}})] - E_{\text{bind}}(\rho_{\text{central,WD}}, M) , \quad (7)$$

where burning coefficient $E_{\text{IPE}} = 1.61 \text{ foe}/M_{\odot}$ (1 foe= 10^{51} ergs) is the energy per unit mass of burning CO (with equal amounts of carbon and oxygen) to IPEs, M is the WD/supernova mass in solar mass units, $R = 0.768$ is the fraction of E_{IPE} released by burning CO (with equal amounts of carbon and oxygen) to IMEs, $(1 - f_{\text{CO}} - f_{\text{IPE}}) = f_{\text{IME}}$ from equation (4), $E_{\text{bind}}(\rho_{\text{central,WD}}, M)$ is the binding energy of the progenitor WD, and $\rho_{\text{central,WD}}$ is the central density of the progenitor WD. The value of E_{IPE} is weighted average of the burning coefficients for burning CO (with equal amounts of carbon and oxygen) to ^{56}Ni ($1.56 \text{ foe}/M_{\odot}$) and

an average of stable IPEs ($1.74 \text{ foe}/M_\odot$). The weights for the averaging are 0.7 for ^{56}Ni and 0.3 for the stable IPEs: these weights agree with the our adoption of fiducial $g = 0.7$ (see above). The value of R is obtained by dividing an averaged energy per unit mass of burning CO (with equal amounts of carbon and oxygen) to IMEs ($1.24 \text{ foe}/M_\odot$) by $1.61 \text{ foe}/M_\odot$. The burning coefficient values $1.56 \text{ foe}/M_\odot$, $1.74 \text{ foe}/M_\odot$, and $1.24 \text{ foe}/M_\odot$ were taken from Woosley et al. (2006). (Actually, used $E_{\text{IPE}} = 1.55 \text{ foe}/M_\odot$ and $R = 0.76$ which are older value given by Branch (1992). The difference between the older and newer values is negligible for H2006’s analysis.)

The binding energy formula in equation (7) comes from YL and applies to WDs (including super-Chandrasekhar WDs) partially sustained against collapse by rotation. The formula is based on YL’s theory of differential rotation of mass-accreting WDs and is for zero temperature WDs. The effects of finite temperature are small for the purposes of H2006 and the SSC model (which also uses eq. (7): see § 4 and Appendix A). The mean angular velocities of super-Chandrasekhar WD models YL consider are typically of order a few radians per second (see YL’s Tables 1 and 2). The formula is verified for the $\rho_{\text{central,WD}}$ range $\sim 10^8\text{--}10^{10} \text{ g cm}^{-3}$ and the mass range $\sim 1.16\text{--}2.05 M_\odot$. We present YL’s binding energy formula and ancillary formulae for reference in Appendix B.

The $\rho_{\text{central,WD}}$ range for YL’s binding formula includes the range that can lead to WD explosion. No explosion probably happens for $\rho_{\text{central,WD}} \lesssim 2.5 \times 10^9 \text{ g cm}^{-3}$ (e.g., Woosley et al. 2006) and above $\rho_{\text{central,WD}} \approx 10^{10} \text{ g cm}^{-3}$ the WD will probably experience electron-capture induced collapse to a neutron star for plausible accretion histories rather than explode (Nomoto & Kondo 1991; YL). Woosley et al. (2006) adopt $\rho_{\text{central,WD}} = 2.9 \times 10^9 \text{ g cm}^{-3}$ as their fiducial explosion density based on their explosion modeling experience: we follow them in adopting this density as the fiducial explosion density for most purposes in this paper. The $E_{\text{bind}}(\rho_{\text{central,WD}}, M)$ is approximately linear in mass for a fixed $\rho_{\text{central,WD}}$ (see YL’s Fig. 9). For each $\rho_{\text{central,WD}}$, there are minimum M and E_{bind} which are the mass and binding energy of a non-rotating WD. The minimum M and E_{bind} grow slightly with $\rho_{\text{central,WD}}$ for the range $2.5 \times 10^9\text{--}10^{10} \text{ g cm}^{-3}$: mass from $1.384 M_\odot$ to $1.414 M_\odot$; binding energy from 0.501 foe to 0.570 foe (see eq. (B4) and (B2) in Appendix B). Note that the non-rotating mass range is above the physical Chandrasekhar mass $1.38 M_\odot$. This is because YL use an approximate equation of state for their modeling that gives a Chandrasekhar mass of $1.436 M_\odot$ (see Appendices A and B). The inconsistency with the physical Chandrasekhar mass is small in comparison to the mass variations H2006 and we consider.

YL’s binding energy formula is, in fact, only a close fit to numerical simulations. Those simulations rely on many approximations and YL’s theory of differential rotation in mass-accreting WDs. So YL’s binding energy formula is not the last word in binding energy

formulae. Quantitatively, the binding energy formula is important. If one sets $f_{\text{CO}} = 0.0$ and $f_{\text{IPE}} = 0.5$, which are somewhat realistic for SNe Ia, then the nuclear burning energy part of equation (7) becomes

$$E_{\text{nuc}} = 1.43 \times (M - 1.4) + 2.00 \text{ foe} , \quad (8)$$

where M is solar masses and we have used $M = 1.4 M_{\odot}$ as a fiducial value for this argument since that is approximately the minimum mass for explosion. The binding energy formula can be approximated as a line to high accuracy (Appendix B) with coefficients depending on density. For our fiducial $\rho_{\text{central,WD}} = 2.9 \times 10^9 \text{ g cm}^{-3}$, the binding energy formula is approximated for the mass range $\sim 1.4\text{--}3 M_{\odot}$ (which turns out to be the mass range of interest in this paper) by the least-squares-fit line

$$E_{\text{bind}} \approx 1.220 \times (M - 1.4) + 0.506 \text{ foe} , \quad (9)$$

where M is solar masses and we have again used $M = 1.4 M_{\odot}$ as a fiducial value. Comparing equations (8) and (9), it is clear that the binding energy will always be important to the behavior of the ejecta for the mass range of interest in this paper (which, again, is $\sim 1.4\text{--}3 M_{\odot}$) since the nuclear burning energy is never overwhelmingly dominant for this range. Thus, the quantitative results of H2006’s SN Ia model and the SSC model do depend on the YL’s binding energy formula. But it is likely that improvements to YL’s formula will not change these results qualitatively, unless rotating WDs with masses significantly greater than the Chandrasekhar mass are ruled out by improvements in the input physics of YL’s theory of differential rotation in mass-accreting WDs.

Using the kinetic energy from equation (7) with $\rho_{\text{central,WD}} = 4 \times 10^9 \text{ g cm}^{-3}$ in all cases, H2006 calculate characteristic kinetic-energy velocities using the formula

$$v_{\text{kin}} = \sqrt{\frac{2E}{M}} = 10027 \text{ km s}^{-1} \times \sqrt{\left(\frac{E}{1 \text{ foe}}\right) \left(\frac{M_{\odot}}{M}\right)} , \quad (10)$$

where the second expression was created using $M_{\odot} = 1.9891 \times 10^{33} \text{ g}$ (e.g., Cox 2000, p. 12). H2006’s Figure 4b–c shows curves of v_{kin} versus ^{56}Ni mass ($M_{^{56}\text{Ni}}$) where the curves are for WD masses in the range from $1.4 M_{\odot}$ (i.e., approximately the Chandrasekhar mass: see Appendix A) to $2.1 M_{\odot}$ and a range of f_{CO} values from 0 to 0.3.

For an observation-derived quantity to compare to the v_{kin} curves, H2006 make use of the 26 SNe Ia of the low- z sample. On their Figure 4b–c, H2006 plot Si II $\lambda 6355$ line velocities for the low- z sample for 40 days past B maximum calculated from a least-squares fit to the line velocity evolutions which in some cases extend to 40 days or a bit more past B maximum (Benetti et al. 2005). If the composition change between the IPE core and silicon-sulfur layer

above the IPE core is reasonably sharp (as explosion models suggest: e.g., model W7), then the Si II $\lambda 6355$ line velocity of a SNe Ia should stop decreasing (we can say it plateaus) at about the velocity of the IPE-core boundary (which we call the IPE-core velocity for brevity) since the line formation for silicon and other IME P Cygni lines cannot recede into the IPE core where there is almost no IME matter to cause IME line formation. This plateauing of the Si II $\lambda 6355$ line velocity may well have happened in some of the low- z sample as is suggest by the data from about 40 days past B maximum (Benetti et al. 2005, Fig. 1). Unfortunately, line blending with iron lines that develop after B maximum may change the Si II $\lambda 6355$ line velocity away from being just the IPE-core velocity. Nevertheless, the long-post- B -maximum Si II $\lambda 6355$ line velocities (when the Si II $\lambda 6355$ line can be identified) may be a good approximation to the IPE-core velocity. We discuss determination of the IPE-core velocities further in § 3.

H2006 use the slope of the best fit line of that member of the low- z sample that is closest to SN 2003fg on a plot of near- B -maximum Si II $\lambda 6355$ line velocity versus $M_{56\text{Ni}}$ (H2006’s Fig. 4a) to extrapolate from their SN 2003fg 2-day-past- B -maximum Si II $\lambda 6355$ line velocity to a 40-days-past- B -maximum Si II $\lambda 6355$ line velocity for SN 2003fg. They plot this on their Figure 4b–c along with the low- z sample 40-days-past- B -maximum Si II $\lambda 6355$ line velocities. Taking their Figure 4b–c at face value, except for SN 2003fg, all the SNe Ia from the low- z sample fall in their figure in the range where a near-Chandrasekhar mass is favored or cannot be excluded if f_{CO} is high. (The higher f_{CO} , the lower f_{IME} low) and the less energy from nuclear burning, and so the lower characteristic kinetic-energy velocity without having to invoke extra mass beyond the Chandrasekhar mass to slow the ejecta down.) If f_{CO} is low (or f_{IME} high), some of these SNe Ia may be super-Chandrasekhar with masses up to $\sim 2 M_{\odot}$ again taking H2006’s Figure 4b–c at face value.

SN 2003fg is well away from the low- z sample and is clearly in the super-Chandrasekhar mass region with mass $\gtrsim 2 M_{\odot}$ for $f_{\text{CO}} \lesssim 0.2$. As discussed in § 1, it is probable that normal SNe Ia have $f_{\text{CO}} \lesssim 0.07$ and, in the context of energy production from the nuclear burning of CO, 0.07 is much less than 0.2. The spectrum of SN 2003fg does show a possible multiplet C II $\lambda 4267$ P Cygni line (e.g., Wiese et al. 1966, p. 39) that has hitherto been only very tentatively identified in SN Ia spectra (Branch et al. 2003) and would be expected to be weaker in local-thermodynamic equilibrium (LTE) than C II lines that have been tentatively identified in SN Ia spectra. Those other C II lines may be hidden in the noise of the SN 2003fg spectra. If the C II line identification is correct, it suggests SN 2003fg may have a larger than normal unburnt CO abundance in its outer layers. But given the overall normality of the SN 2003fg spectrum, $f_{\text{CO}} \lesssim 0.2$ is probable. Thus, from H2006’s Figure 4b–c, one would find the SN 2003fg mass to be $\gtrsim 2 M_{\odot}$. Given the conclusion of Langer et al. (2000) that WD masses much greater than $\sim 2 M_{\odot}$ are not attainable in possible accretion histories,

H2006’s Figure 4b–c suggests a SN 2003fg mass of $\sim 2 M_{\odot}$.

Unfortunately, as H2006 emphasize the comparison of 40-days-past-*B*-maximum Si II $\lambda 6355$ line velocities and characteristic kinetic-energy velocity is ambiguous. The characteristic kinetic-energy velocity has no definite theoretical relation to the line velocities or the IPE-core velocities that the line velocities probably approximate. Thus, the comparison on their Figure 4b–c must be regarded as only suggestive. But the fact that SN 2003fg is so far away from the other SNe Ia on the plot and well into the super-Chandrasekhar mass region is striking.

Taken altogether the arguments above give reasonable evidence that SN 2003fg had a super-Chandrasekhar mass which is perhaps $\sim 2 M_{\odot}$. One would like, however, a more reliable quantitative value for the SN 2003fg mass or at least more robust lower bounds on this mass. In § 4, we introduce a simple model (the SSC model) which is an improvement on the model of H2006 and which gives lower bounds on the SN 2003fg mass of varying confidence.

3. THE IPE-CORE BOUNDARY AND THE IPE-CORE VELOCITY

Before going on to the SSC model, some further discussion of IPE-core boundary and IPE-core velocity (see § 2) needs to be made to support the validity of approximating the IPE-core boundary as perfectly sharp in the SSC model (see § 4) and to relate the IPE-core velocity to more directly observable quantities.

The existence of a relatively sharp boundary for the IPE core for normal SNe Ia at least is basically supported by spectrum modeling using explosion models. Typically in useful SN Ia explosion models, the IPEs fall from dominating the composition (nearly 100% of the composition by mass) to being a trace (a few percent by mass) over a few thousands of kilometers per second in velocity coordinate. For example, the dominance-to-trace transition in the partially successful models W7 (Nomoto et al. 1984; Thielemann et al. 1986) and DD4 (a well-known delayed-detonation model) (Woosley 1991) happens in the range ~ 8500 – 11000 km s^{-1} . The overall SN Ia ejecta velocity scale is $\sim 25000 \text{ km s}^{-1}$ or more, and so assuming a perfectly sharp boundary is reasonable in a simple model. We must add, however, that some mixing or explosion-synthesis of IPEs beyond the IPE-cores of explosion models is sometimes helpful in SN Ia spectrum modeling (Baron et al. 2006). We will not consider this complication further in this paper it should be kept in mind for future work.

Since the IPE-core boundary is not perfectly sharp, one needs a definition for the characteristic IPE-core velocity. Probably the most sensible definition of the characteristic IPE-core

velocity for explosion models is the velocity of the spherical shell that would just contain all the explosion-synthesized IPEs and nothing else given the model comoving density profile. For model W7, this velocity is 9800 km s^{-1} which just $\sim 200 \text{ km s}^{-1}$ less than the velocity where the mass fractions of ^{56}Ni and silicon are about equal. For a quick survey, we therefore adopt the velocity of equality of ^{56}Ni and silicon mass fractions as an adequate proxy for the IPE-core velocity. For some models that have been found useful in analyzing SNe Ia, the equality velocities fall in the range $\sim 7000\text{--}13000 \text{ km s}^{-1}$ (e.g., Nomoto et al. 1984; Thielemann et al. 1986; Woosley 1991; Khokhlov et al. 1993; Höflich et al. 1998). For the low- z sample, most of the calculated Si II $\lambda 6355$ line velocities for 40 days past B maximum are in the range $\sim 8000\text{--}11000 \text{ km s}^{-1}$ either by measurement or extrapolation: the five faint SNe Ia have lower Si II $\lambda 6355$ line velocities in the range $\sim 5000\text{--}8000 \text{ km s}^{-1}$ either by measurement or extrapolation (Benetti et al. 2005). (Faint SN Ia is a classification of citetbenetti for those SNe Ia that are distinctly fainter than normal SNe Ia: the prototypes of this classification are SN 1986G and SN 1991bg.) The 40-day-past- B -maximum values for the non-faint SNe Ia are roughly consistent with equality velocities we cite and support the idea that the long-post- B -maximum Si II $\lambda 6355$ line velocities at least for non-faint SNe Ia approximate the IPE-core velocities. Recall that some of these 40-day-past- B -maximum Si II $\lambda 6355$ line velocities seem to be plateauing (Benetti et al. 2005, Fig. 1).

Besides the Si II $\lambda 6355$ line, other IME P Cygni lines are useful in locating or at least constraining the IPE-core velocity. For example, the resonance multiplet Na I $\lambda 5892$ and calcium multiplets Ca II $\lambda 3945$ (resonance) and Ca II $\lambda 8579$ (non-resonance, but arising from a metastable level) (e.g., Wiese et al. 1969, p. 2, 252, 251) give rise to P Cygni profiles that can persist to 100 days or more past B maximum and, in the core normal SN Ia SN 1994D (e.g., Branch et al. 2005) for example, have line velocities $\sim 11000 \text{ km s}^{-1}$, $\sim 8000 \text{ km s}^{-1}$, and $\sim 10000 \text{ km s}^{-1}$, respectively, at 115 days past B maximum. In the ultraviolet, the P Cygni line of resonance multiplet Mg II $\lambda 2798$ (e.g., Wiese et al. 1969, p. 30) also seems long persistent (Kirshner et al. 1993; Ruiz-Lapuente et al. 1995) with a line velocity that seems to stay $\gtrsim 14000 \text{ km s}^{-1}$ to 291 days past B maximum although line-blending with IPE lines makes it hard to be sure that this velocity is representative of the magnesium layer. The Mg II $\lambda 2797.9$ region of the ultraviolet is rarely observed for low- z supernovae (because the observation requires space-based telescopes which are not always available), but for high- z ones the Mg II $\lambda 2797.9$ region can be redshifted into more readily observed wavelength ranges. H2006’s spectrum of SN 2003fg almost extends far enough to the blue to see the region of the Mg II $\lambda 2797.9$ line. The late, persistent IME P Cygni lines with relatively high line velocities suggest that the line formation layers for these lines has receded to the vicinity of or some point above the IPE core and then plateaued since there is almost no IME matter in the IPE core for lower velocity IME line formation. Thus, the sodium, magnesium, and

calcium line velocities may constrain the IPE-core velocity. On the theoretical side, explosion models suggest that the abundances of sodium, magnesium, and calcium all decline going inward in the ejecta. For model W7, sodium, magnesium, and calcium fall below their solar mass fractions 3.2×10^{-5} , 6.0×10^{-4} , and 5.7×10^{-5} , respectively, (Asplund et al. 2005) at velocities $\sim 14500 \text{ km s}^{-1}$, $\sim 13000 \text{ km s}^{-1}$, and $\sim 9000 \text{ km s}^{-1}$, respectively. These velocities are only representative, of course, but they also suggest that the lowest observed line velocities for Na I $\lambda 5892$, Mg II $\lambda 2798$, Ca II $\lambda 3945$, Ca II $\lambda 8579$ for a SN Ia could constrain the IPE-core velocity. Recall from above, that for model W7 the characteristic IPE-core velocity is $\sim 9800 \text{ km s}^{-1}$.

Besides P Cygni lines, one can also consider for the determination of the IPE-core boundary the forbidden Fe II and Fe III emission lines that dominate the optical SN Ia spectrum in the nebular phase when the ejecta become optically thin. Modeling these emission lines can be used to constrain the IPE-core velocity. Current results suggest IPE-core velocities in the range $\sim 7500\text{--}10500 \text{ km s}^{-1}$ for normal and somewhat bright SNe Ia and IPE-core velocities of $\sim 2000 \text{ km s}^{-1}$ for very faint SNe Ia like SN 1991bg (Mazzali et al. 1998). Note that the calculations for these IPE-core velocities apparently assumed a uniform density for the IPE core (as by Mazzali et al. (1997)) which a significant approximation.

The above discussion shows both from explosion models and observations that something like a sharp IPE-core boundary does exist, a characteristic IPE-core velocity can be defined, and that this characteristic IPE-core velocity is in practice determinable to within some uncertainty.

4. THE SSC MODEL FOR SUPER-CHANDRASEKHAR-MASS SNe Ia

In this section, we introduce a model for studying super-Chandrasekhar-mass SNe Ia that is an improvement on the model of H2006. We call this model the SSC model for Simple Super-Chandrasekhar model for SNe Ia. The progenitor for the model is, as in the standard SN Ia model, a mass-accreting CO WD. The SSC model has 3 components. The first component is equation (7) (§ 2) (slightly rewritten: see below) to determine the total energy of the SN Ia ejecta. Because we use this equation, we assume we can approximate ejecta as consisting of only three types of material for the kinetic energy calculation: explosion-synthesized IPEs, explosion-synthesized IMEs, and unburnt CO. By using equation (7), we are, of course, also assuming that the progenitor WD is rotating for masses significantly greater than the physical Chandrasekhar mass $1.38 M_{\odot}$ (see Appendix A) and we are relying on YL’s binding energy formula for rotating WDs. As discussed in § 2 our results from the SSC model quantitatively depend on YL’s binding energy formula. Qualitatively, the results

from the SSC model are probably robust.

The second component of the SSC model is the exponential model of the ejecta (Jeffery 1999) which is explained as follows. Recall from § 1 that after very early times supernovae are in homologous expansion where velocity becomes a good comoving frame coordinate and all mass element densities scale as t^{-3} . Now as has been known for some time, many partially successful SN Ia models (e.g., model W7) have comoving density profiles that are approximately inverse exponentials of velocity, (Jeffery et al. 1992). (Even earlier, it was recognized that the comoving density profiles of core-collapse supernova models were sometimes approximately piecewise inverse exponentials with velocity (Pizzochero 1990).) Making use of homologous expansion and the (inverse) exponential density profile approximation, one obtains a useful parameterization of approximate SN Ia density profiles:

$$\rho(v, t) = \rho_{\text{central},0} \left(\frac{t_0}{t} \right)^3 \exp \left(-\frac{v}{v_e} \right), \quad (11)$$

where t_0 is some fiducial time, $\rho_{\text{central},0}$ is the central density of the ejecta at the fiducial time, and v_e is the e -folding velocity. For examples of SN Ia model profiles that approximate exponentials see, e.g., Dwarkadas & Chevalier (1998, Fig. 1), Baron et al. (2006, Fig. 11), and Woosley et al. (2006, Fig. 4). It is straightforward to show that

$$v_e = \sqrt{\frac{1}{6} \frac{E}{M}} = 2894.7 \text{ km s}^{-1} \times \sqrt{\left(\frac{E}{1 \text{ foe}} \right) \left(\frac{M_\odot}{M} \right)}, \quad (12)$$

where, as in § 2, E is the ejecta kinetic energy and M is the ejecta mass (Jeffery 1999). Since SN Ia kinetic energy should be of order a foe and mass of order M_\odot , the coefficient of the second expression of equation (12) can be take as a good fiducial value for the SN Ia e -folding velocities. To support this we can consider model W7. Using the E and M values for model W7 in equation (12) gives $v_e = 2670 \text{ km s}^{-1}$ which is not far from 2894.7 km s^{-1} and which, in fact, leads to a good fit to the model W7 density profile: see the URL given in footnote 2 for plots showing this fit. We note that the characteristic kinetic-energy velocity defined by equation (10) (§ 2) is related to v_e by

$$v_{\text{kin}} = \sqrt{12} v_e. \quad (13)$$

It is also straightforward to show that the fraction of ejecta mass, f , interior to reduced velocity

$$x = \frac{v}{v_e} \quad (14)$$

is given by

$$f = \begin{cases} \left[1 - \exp(-x) \left(1 + x + \frac{1}{2}x^2 \right) \right] & \text{in general;} \\ \left\{ 1 - \exp(-x) \left[\exp(x) - \sum_{k=3}^{\infty} \frac{x^k}{k!} \right] \right\} & \text{in general;} \\ \frac{x^3}{6} - \frac{x^4}{8} + \frac{x^5}{20} & \text{to 5th order in small } x; \\ 0.080301397071394\dots & \text{for } x = 1; \\ 0.67246197033808\dots \approx \frac{2}{3} & \text{for } x = \sqrt{12} = 3.4641016151377\dots; \\ 0.99723060428448\dots & \text{for } x = 10 \end{cases} \quad (15)$$

(Jeffery 1999).

Note that the exponential density profile extends to infinite velocity, in principal. Obviously, the approximation of an exponential density profile must fail as velocity becomes relativistic. For modeling SNe Ia, this is not a problem since there is seldom need to invoke matter beyond $\sim 30000 \text{ km s}^{-1}$ ($\beta \approx 0.100$) and matter at $\sim 40000 \text{ km s}^{-1}$ ($\beta \approx 0.133$) may be the highest ever needed (Jeffery et al. 1992). For such velocities, relativistic effects are small since they mostly go as β^2 . Using our fiducial value $v_e = 2894.7 \text{ km s}^{-1}$, the reduced velocity corresponding to 30000 km s^{-1} is ~ 10 . From equation (15), $f(10) \approx 0.997$. Thus, in modeling with exponential density profiles, typically much less than 1% of the ejecta will be put at velocities where relativistic effects are important. Therefore, typical relativistic effects are going to be negligible when using exponential density profiles.

As a semi-necessary adjunct to assuming an exponential density profile, we also assume that the ejecta can be approximated as spherically symmetric. This is a reasonable simplifying assumption, but is not necessarily completely valid. Because of their homogeneity, normal SNe Ia are probably quite spherically symmetric: even identical SNe Ia would look significantly different from different viewing directions if they were significantly aspherical. There is, however, some evidence from spectropolarimetry for departures from spherical symmetry for both normal SNe Ia (Wang et al. 2003) and peculiar SNe Ia (Howell et al. 2001). Thus, a priori, one cannot rule out significant asymmetry for any particular SN Ia especially if it is unprecedented like SN 2003fg. Moreover, if the progenitor of SN 2003fg was indeed rotating and this accounts for its probable super-Chandrasekhar mass, then its progenitor could have been quite aspherical. The ratio of polar to equatorial radii for YL’s rotating WD models fall as low as ~ 0.3 for masses of $\sim 2 M_{\odot}$ (see YL’s Tables 1 and 2). The explosion of such asymmetric WDs may, however, reduce the asymmetry of the matter considerably (YL). For the present, assuming spherical symmetry for the ejecta is justified by simplicity and the lack of any evidence that SN 2003fg shows any asymmetry.

The third component of the SSC model is to assume that a well-defined IPE core exists with a boundary that we can approximate as absolutely sharp and that we can make the approximation that all explosion-synthesized IPE matter is within the IPE core and no other elements are. This approximation is reasonable as discussed in § 3.

Following a similar path to H2006, we take ejecta mass M , IPE-core mass $M_{\text{IPE-core}}$, a new parameter h , and $\rho_{\text{central,WD}}$ as 4 independent parameters. The new parameter h is given by

$$h = \frac{f_{\text{IME}}}{f_{\text{CO}} + f_{\text{IME}}} . \quad (16)$$

We prefer h as an independent parameter rather than f_{CO} adopted by H2006 or f_{IME} which could also be used. One can obtain f_{CO} and f_{IME} from h and f_{IPE} (which is obtained from equation (4) (§ 2) using M and $M_{\text{IPE-core}}$) using the formulae

$$f_{\text{CO}} = (1 - h)(1 - f_{\text{IPE}}) \quad \text{and} \quad f_{\text{IME}} = h(1 - f_{\text{IPE}}) . \quad (17)$$

Using h as an independent parameter makes simpler the use of IPE-core velocity $v_{\text{IPE-core}}$ as an independent parameter in place of M . We want this simplification when we solve for an unknown M given $M_{\text{IPE-core}}$, $v_{\text{IPE-core}}$, h , and $\rho_{\text{central,WD}}$. We find such solutions in § 6 and show how the solutions are done and why h preferred to f_{CO} and f_{IME} as an independent parameter in Appendix C.

For convenient reference and making use of equations (4) (§ 2) and (17), we rewrite the kinetic energy equation (7) (§ 2) in terms of parameter h :

$$E = E_{\text{IPE}}M[f_{\text{IPE}} + Rh(1 - f_{\text{IPE}})] - E_{\text{bind}}(\rho_{\text{central,WD}}, M) . \quad (18)$$

Substituting values for M , f_{IPE} , h , and $\rho_{\text{central,WD}}$ into equation (18), we get the kinetic energy E and then substituting values for M and E into equation (12) gives the e -folding velocity v_e .

Now to determine $v_{\text{IPE-core}}$, we need the reduced IPE-core velocity $x_{\text{IPE-core}}$ which we obtain by solving for $x_{\text{IPE-core}}$ from equation (15) with f set to f_{IPE} . Unfortunately, there is no general analytic solution for x given f for equation (15). In the special cases of $f = 0$ and $f = 1$, the solutions are, respectively, $x = 0$ and $x = \infty$. Otherwise we can solve equation (15) by the Newton-Raphson method (e.g., Press et al. 1992, p. 355ff) for x given f . The Newton-Raphson method is guaranteed to converge in this case since f is monotonically increasing with x and only has a stationary point at infinity provided one prevents the Newton-Raphson corrections from causing overshooting of the diminishing allowed range for the final solution. The derivative of f (which is needed for the Newton-Raphson method solution) is

$$\frac{df}{dx} = \frac{x^2}{2} \exp(-x) . \quad (19)$$

A good initial value for the Newton-Raphson method iteration for $f < 1$ is the 3rd-order-in-small- y solution for x given by

$$x_{3\text{rd}} = y + \frac{1}{4}y^2 + \frac{7}{80}y^3, \quad (20)$$

where $y = (6f)^{1/3}$. This solution for x is about 10% accurate for $f \lesssim 0.33$: it improves in accuracy as $y \rightarrow 0$, of course. Either the 2nd-order-in-small- y or 1st-order-in-small- y solutions for x are almost as good initial values for the iteration for any $f < 1$ as the 3rd-order-in-small- y solution for x . As an alternative to the Newton-Raphson method, one can solve for x using the iteration equation method using an iteration equation obtained from rearranging equation (15). The iteration equation is

$$x_{\text{out}} = \ln \left[\frac{1 + x_{\text{in}} + (1/2)x_{\text{in}}^2}{1 - f} \right], \quad (21)$$

where x_{in} is an input x value and x_{out} is an output x value. The iteration is guaranteed to converge since the derivative $|dx_{\text{out}}/dx_{\text{in}}| \leq 1$ with the equality holding only for $x_{\text{in}} = 0$ which is a point that can be avoided since we already know that $x = 0$ for $f = 0$. In practice, the iteration equation solution to reasonable convergence takes about 50% longer in CPU time than the Newton-Raphson method. One can obtain a reasonable approximate analytic solution for x , x_{approx} , by substituting $x_{3\text{rd}}$ from equation (20) into the iteration equation. This approximate analytic solution is given by

$$x_{\text{approx}} = \ln \left[\frac{1 + x_{3\text{rd}} + (1/2)x_{3\text{rd}}^2}{1 - f} \right]. \quad (22)$$

The approximate analytic solution is always an underestimate with a maximum relative error of $\sim 19\%$ for $f \approx 0.995$: the relative error decreases with f increasing or decreasing from $f \approx 0.995$ and it goes to zero in the limits $f \rightarrow 0$ and $f \rightarrow 1$. More elaborate analytic formulae can give better accuracy for x than equation (22): e.g., substituting x_{approx} itself into equation (22) instead of $x_{3\text{rd}}$ gives a significantly more accurate approximate analytic formula for x . By whatever means, having obtained an accurate $x_{\text{IPE-core}}$, we obtain the IPE-core velocity from

$$v_{\text{IPE-core}} = x_{\text{IPE-core}} v_e. \quad (23)$$

H2006 in their analysis (see § 2) compared 40-days-past- B -maximum-light Si II $\lambda 6355$ line velocities to v_{kin} . As we argued in § 2 and § 3, the long-past- B -maximum-light Si II $\lambda 6355$ line velocity is a reasonable approximation to the IPE-core velocity. As H2006 acknowledged, their comparison was ambiguous because there is no necessary theoretical connection between the long-past- B -maximum-light Si II $\lambda 6355$ line velocity and v_{kin} . The situation is further

clarified by the SSC model, where it is clear that there is no necessity for $v_{\text{IPE-core}}$ to equal v_{kin} even approximately although it could do so. If we set $v_{\text{IPE-core}}$ to v_{kin} (i.e., $x_{\text{IPE-core}} = \sqrt{12}$), then f_{IPE} would be fixed at $0.6724619703381 \approx 2/3$ as we see from equation (15). However, in the SSC model we are free to vary f_{IPE} from 0 to 1 provided that $E \geq 0$ which is necessary for the WD to explode.

We illustrate the behavior of the SSC model in Figures 1 and 2 by plotting $v_{\text{IPE-core}}$ as a function of $M_{\text{IPE-core}}$ for representative values of the 3 other independent parameters (i.e., mass M , h , and $\rho_{\text{central,WD}}$) which are held constant for each curve. (The data points on the figures are discussed in §§ 5 and 6.) Recall from § 2 that the $\rho_{\text{central,WD}}$ range $\sim 2.5 \times 10^9$ – $10^{10} \text{ g cm}^{-3}$ is believed to be the allowed range for WD explosions and that our fiducial $\rho_{\text{central,WD}} = 2.9 \times 10^9 \text{ g cm}^{-3}$. To explore the possible $\rho_{\text{central,WD}}$ range for SN Ia progenitors, we used the fiducial $\rho_{\text{central,WD}} = 2.9 \times 10^9 \text{ g cm}^{-3}$ (which is not far from the low end of the range) for the Figure 1 calculations and $\rho_{\text{central,WD}} = 10^{10} \text{ g cm}^{-3}$ for the Figure 2 calculations. Most explosion modelers find $\rho_{\text{central,WD}}$ much closer to the low end of the allowed range for plausible explosions (e.g., Nomoto et al. 1984; Thielemann et al. 1986; Khokhlov et al. 1993; Woosley & Weaver 1994; Höflich & Khokhlov 1996; Höflich et al. 1998): thus $\rho_{\text{central,WD}} = 10^{10} \text{ g cm}^{-3}$ is actually an extreme upper limit and a WD that evades an explosion and gets to this limit is probably on the verge of collapse to a neutron star (Nomoto & Kondo 1991; YL). The binding energy increases with central density (see YL’s Fig. 9), and so all other things being equal, increasing density leads to lower $v_{\text{IPE-core}}$. This is why the curves in Figure 2 are generally lower than their counterparts in Figure 1.

The solid curves (which form cornucopias) are for $h = 1$ which means $f_{\text{IME}} = 1 - f_{\text{IPE}}$, $f_{\text{CO}} = 0$, and there are only IMEs above the IPE core. The mass in solar mass units for each solid curve is given at the upper right end of the curve: the masses run from $1.388 M_{\odot}$ for Figure 1 and $1.414 M_{\odot}$ for Figure 2 to $3 M_{\odot}$ in increments of $0.1 M_{\odot}$ for $M \geq 1.5 M_{\odot}$. The masses $1.388 M_{\odot}$ and $1.414 M_{\odot}$ are the masses for non-rotating WDs from YL’s equation (22) (see also eq. (B4) in Appendix B) for the input $\rho_{\text{central,WD}}$ values and we just label their curves by M_{NR} on the figures. The non-rotating WD masses are the lower bounds on the masses for the input $\rho_{\text{central,WD}}$ values and are near the physical Chandrasekhar mass $1.38 M_{\odot}$ (see Appendix A). As mentioned in § 2, the non-rotating WD masses can slightly exceed the physical Chandrasekhar mass $1.38 M_{\odot}$. This is because YL use an approximate equation of state for their modeling that gives a Chandrasekhar mass of $1.436 M_{\odot}$ (see Appendices A and B). This inconsistency from the physical Chandrasekhar mass is small in comparison to the mass variations we are considering. Actually all the masses we discuss probably have uncertainties of a few percent for the given input parameters because they are based on YL’s choice of equation of state: they are probably mostly slightly larger than the input parameters would imply with a more accurate equation of state (see Appendix A). For

clarity, we call the $1.388 M_{\odot}$ and $1.414 M_{\odot}$ mass curves the M_{NR} mass curves.

The general behavior of the solid curves can be explained as follows. In regard to varying mass M for a given IPE-core mass, the smaller M is, the higher $v_{\text{IPE-core}}$ tends to be since the WD binding energy decreases with decreasing M , there is less mass to accelerate, $v_{\text{IPE-core}}$ moves to a higher mass fraction in the ejecta, and the nuclear burning energy decreases rather weakly only through decreasing amount of burning to IMEs. This explains why as curve mass decreases, the curves move upward. In overall curve appearance, the curves move toward the upper left as mass decreases. In regard to varying $M_{\text{IPE-core}}$ for fixed M , as $M_{\text{IPE-core}}$ increases, $v_{\text{IPE-core}}$ increases monotonically. There are two causes for this. First, as one moves outward in mass fraction with everything fixed, ejecta velocity will increase since outer matter must move faster than inner matter. Second if as one moves outward in mass fraction and the IPE-core boundary moves with you, there is more kinetic energy than otherwise to drive the outer layers. Both causes help $v_{\text{IPE-core}}$ to increase monotonically with $M_{\text{IPE-core}}$. Note that the solid curves all begin at $M_{\text{IPE-core}} = 0$ since burning all the non-IPE-core matter to IMEs always ensures adequate energy for a WD explosion. The solid curves also begin at $v_{\text{IPE-core}} = 0$ since that is the limiting IPE-core velocity when there is no IPE core.

The dotted curves are for $h = 0$ which means $f_{\text{IME}} = 0$, $f_{\text{CO}} = 1 - f_{\text{IPE}}$, and there is only unburnt CO above the IPE core. As mentioned in § 1, the spectra of all SNe Ia, including SN 2003fg, are dominated by IME lines at least in the early-post- B -maximum phase, and so we know that there must be abundant IMEs in the outer layers of all SN Ia ejecta. Partially successful explosion models also yield abundant IMEs: for example, Model W7 gives $f_{\text{IME}} = 0.281$ and $h = 0.798$ (Thielemann et al. 1986); example delayed-detonation models give $h \gtrsim 0.95$ (Khokhlov et al. 1993; Höflich et al. 1998). Thus, 0 must be regarded an extreme lower limit on h . However, as discussed in § 2, SN 2003fg may have had more unburnt CO than normal SNe Ia, and so h may be significantly less than 1 for SN 2003fg. Thus, the $h = 0$ curves are relevant to this study.

The masses for the dotted curves are the same as for the solid curves and dotted curves are ordered in the same way as the solid curves by mass: the dotted curves are labeled by mass at their low IPE-core mass end. On Figure 2 the dotted curves for masses greater than $2.8 M_{\odot}$ are off the figure. Since there is no burning of IMEs for the dotted curves, they represent models with less energy than the counterpart solid curves. Thus, $v_{\text{IPE-core}}$ values for the dotted curves at a given $M_{\text{IPE-core}}$ are always less than that for the counterpart solid curves at the same $M_{\text{IPE-core}}$. The dotted curves all begin at zero IPE-core velocity and at non-zero IPE-core mass. In the case of the dotted curves, the IPE core must reach a sufficient size before there is enough nuclear burning energy to unbind the WD: recall there

is no burning of matter outside of the IPE core in the case of these curves. The behaviors of the dotted curves as M is varied for fixed $M_{\text{IPE-core}}$ and as $M_{\text{IPE-core}}$ is varied for fixed M have essentially the same explanation as for the solid curves.

As $M_{\text{IPE-core}}$ grows for a constant M , the relative amounts of IMEs and CO become less important for the energetics, and thus the dotted curves converge toward their counterpart solid curves as $M_{\text{IPE-core}}$ grows large. For the counterpart dotted and solid curves for larger M , close convergence occurs off the top or right edges of the figures. Final convergence, of course, happens in the limit of $M_{\text{IPE-core}} \rightarrow M$ which causes $v_{\text{IPE-core}}$ to go to the unphysical limit of infinity. Non-relativistic physics fails long before this velocity limit is reached. Since the figures only show up to 13000 km s^{-1} (which is $\beta \approx 0.0434$), the region where non-relativistic physics fails occurs well off the figures for all the curves.

We need to emphasize that YL have only verified their binding energy formula for the mass range $\sim 1.4\text{--}2.05 M_{\odot}$, and thus we have made a large extrapolation of the usage of binding energy formula in plotting curves for masses up to $3 M_{\odot}$.

5. COMPARING THE SSC MODEL AND OBSERVATIONS OF THE LOW- z SAMPLE OF SNe Ia

The circle points on Figures 1 and 2 are for the low- z sample of SNe Ia from Benetti et al. (2005) which was discussed in § 2. The + points are discussed below, and the letters N, O, X, and Y are for SN 2003fg and are discussed in § 6. The IPE-core masses for the circle points were determined using equation (6) with the $L_{\text{bol}}/\dot{E}_{56\text{Ni}}(t_{\text{bol}})$ values of H2006, $\alpha = 1.2$ (as adopted by H2006 and which we take to be fiducial for this paper), and $g = 0.7$ (which, following H2006, we argued was a good representative fiducial value in § 2). The IPE-core masses are in the range $\sim 0.04\text{--}0.86 M_{\odot}$. The velocities are the Si II $\lambda 6355$ line velocities from 35 days past B maximum derived using the least-squares line fits of Benetti et al. (2005). The velocities are in the range $\sim 5900\text{--}11200 \text{ km s}^{-1}$. As mentioned in § 2, the uncertainties of $L_{\text{bol}}/\dot{E}_{56\text{Ni}}(t_{\text{bol}})$ for the low- z sample are in general greater than for SN 2003fg because some of these SNe Ia are not well out in the Hubble flow. We will neglect this complication in our analysis for simplicity and since we are primarily just interested in overall behavior of the low- z sample when analyzed using the curves on Figures 1 and 2.

We prefer 35 days past B maximum to H2006’s 40 days past B maximum in calculating the Si II $\lambda 6355$ line velocities to be used in comparison to the SSC model curves. The reasoning is that after about 35 days past B maximum the derived values in most cases would be extrapolations of uncertain quality of the Si II $\lambda 6355$ line velocity curves (Benetti

et al. 2005, Fig. 1). Also some of the Si II $\lambda 6355$ line velocity curves seem to be plateauing at about 35 days past B maximum (Benetti et al. 2005, Fig. 1) which suggests that the Si II $\lambda 6355$ line formation layer has stopped receding into the ejecta because it has receded to the boundary of IPE core and there is no significant silicon below that layer. Thus, the 35-days-past- B -maximum values may in many cases best approximate the IPE-core velocities and this is what we hope the long-past- B -maximum Si II $\lambda 6355$ line velocities will approximate.

The Si II $\lambda 6355$ line velocity of SN 1991bg may still be decreasing at 35 days past B maximum which is about as far as the data of Benetti et al. (2005) go, and so SN 1991bg’s 35-day-past- B -maximum Si II $\lambda 6355$ line velocity is only an upper limit on the IPE-core velocity. From modeling, Mazzali et al. (1998) found that the IPE-core velocity of SN 1991bg was $\sim 2000 \text{ km s}^{-1}$. SN 1991bg is one of the 5 SNe Ia designated as faint by Benetti et al. (2005) in the low- z sample. These faint SNe Ia have the lowest IPE-core masses, and so give the leftmost circle data points on Figures 1 and 2. In order of increasing IPE-core mass on Figures 1 and 2, the faint SNe Ia are: SN 1999by, SN 1991bg, SN 1997cn, SN 1986g, and SN 1993H. The situation for the Si II $\lambda 6355$ line velocities of the other faint SNe Ia are not as clear as for SN 1991bg, but their day-35-past- B -maximum Si II $\lambda 6355$ line velocities are more likely to be only upper bounds on the IPE-core velocities than is the case for the other SNe Ia in the low- z sample.

The circle points are rather dispersed and do not lie along the M_{NR} mass curves. Some are to the right of the M_{NR} mass curves which suggests the possibility that they are for slightly super-Chandrasekhar SNe Ia. But this is very uncertain. The circle points to the left of the M_{NR} mass curves are not to be taken for (significantly) sub-Chandrasekhar SNe Ia. A mechanism for sub-Chandrasekhar SNe Ia has been proposed (Livne & Glasner 1990, 1991), but this mechanism has been ruled out. Explosion models produced using the mechanism led to synthetic lightcurves (Höflich & Khokhlov 1996) and spectra (Nugent et al. 1997) that failed to match observations: among other things the synthetic lightcurves and spectra were too blue. Thus, the circle points to the left of the M_{NR} mass curves are all likely to be from near-Chandrasekhar (or less likely somewhat super-Chandrasekhar) SNe Ia. The main explanation for the deviations of the circle points from the M_{NR} mass curves is likely that α is not 1.2 in general. The faint group of SNe Ia may also deviate significantly from the M_{NR} mass curves because their day-35-past- B -maximum Si II $\lambda 6355$ line velocities are not close upper bounds on their IPE-core velocities. Of course, the SSC model may also be somewhat inadequate for real SNe Ia and/or the g factor may vary significantly from the fiducial 0.7 value.

The reason for believing it is varying α that leads to the dispersion of the circle points

from the M_{NR} mass curves is, as discussed in § 2, that there is reason to believe that α can have a large range: recall that the modeling results of Höflich & Khokhlov (1996) suggest a range of 0.62–1.46 for α . We can derive a semi-empirical range for α , by varying α for the low- z sample such that all the points lie on the M_{NR} mass curves. The range is semi-empirical because we are relying on observations and on the SSC model in the non-rotating mass limit. The range is based on the assumption that most SNe Ia have nearly the Chandrasekhar mass (which is approximated by M_{NR} in the SSC model). We will only do the variation for the M_{NR} mass curves for $h = 1$ since this is likely to be closer to the truth for normal SNe Ia than curves for $h = 0$ (see § 4). The + points on Figures 1 and 2 are the result of varying α . Note that $\alpha < 1.2$ moves points to larger IPE-core mass and $\alpha > 1.2$ moves points to smaller IPE-core mass. The range for α is 0.13–1.72 for Figure 1 and 0.13–1.67 for Figure 2. If we exclude the five faint SNe Ia for which the day-35-past- B -maximum Si II $\lambda 6355$ line velocities are more likely to be only upper bounds on the IPE-core velocities than for the other SNe Ia, we find the α ranges to be 0.68–1.72 for Figure 1 and 0.65–1.67 for Figure 2. Given the assumptions that the SSC model is valid, the non-faint SNe Ia in the low- z sample have day-35-past- B -maximum Si II $\lambda 6355$ line velocities are nearly the IPE-core velocities, the g factor is 0.7, $h \approx 1$, and that none of the low- z sample is significantly super-Chandrasekhar (nor sub-Chandrasekhar), then the semi-empirical α range can be taken as ~ 0.6 –1.7. This α range is plausible given the results of Höflich & Khokhlov (1996), but it is not definitive, of course. If we used the $h = 0$ curves instead of the $h = 1$ curves, the semi-empirical range for α would shift to lower values.

6. COMPARING THE SSC MODEL TO THE SN 2003fg OBSERVATIONS

We now turn our attention to comparing the SSC model to the SN 2003fg observations. In the case of SN 2003fg, we cannot adequately determine the day-35-past- B -maximum Si II $\lambda 6355$ line velocity given only the near- B -maximum Si II $\lambda 6355$ line velocity of $8000 \pm 500 \text{ km s}^{-1}$. Therefore, we will only adopt 8000 km s^{-1} as an upper bound on the IPE-core velocity. The points N, O, X (partially overlapping with O), and Y on Figures 1 and 2 are all SN 2003fg IPE-core velocity upper bound points of 8000 km s^{-1} . As Figures 1 and 2 show, since we can only set an upper bound on the SN 2003fg IPE-core velocity, we can only set a lower bound on the SN 2003fg mass.

Unfortunately in trying to set such a lower bound on SN 2003fg mass, there is no secure way to estimate the IPE-core mass $M_{\text{IPE-core}}$ (which is a SSC model parameter) primarily because of the dispersion in α and secondarily because we can only estimate the g factor. Recall $M_{\text{IPE-core}}$ is calculated from equation (6) in § 2 using g and α and H2006’s

$L_{\text{bol}}/\dot{E}_{^{56}\text{Ni}}(t_{\text{bol}})$ value $1.55 M_{\odot}$ which we assume to have negligible uncertainty. The values of the SSC model parameters $\rho_{\text{central,WD}}$ and h are also not fully constrained. Therefore, we calculate lower bound masses varying the four parameters $\rho_{\text{central,WD}}$, g , α , and h from what we believe to good representative fiducial values to what we believe to be extreme values which tend to minimize the lower bound masses. (Recall, they will be lower bound masses because 8000 km s^{-1} which we use as the input value for $v_{\text{IPE-core}}$ is only an upper bound on $v_{\text{IPE-core}}$.) The fiducial values are $\rho_{\text{central,WD}} = 2.9 \times 10^9 \text{ g cm}^{-3}$ (which we adopted as fiducial in § 2 following Woosley et al. (2006)), $g = 0.7$ (which is certainly good for some SN Ia models: see § 2), $\alpha = 1.2$ (which is good in the sense that it is not extreme: see §§ 2 and 5) and $h = 1$ (which is good for normal SNe Ia given that their spectra up until after B maximum are dominated by IME lines and given that model W7 has $h = 0.798$ (Thielemann et al. 1986) and some example delayed-detonation models have $h \gtrsim 0.95$ (e.g., Khokhlov et al. 1993; Höflich et al. 1998)). The extreme parameter values we consider are $\rho_{\text{central,WD}} = 10^{10} \text{ g cm}^{-3}$ (which is extreme based on the fact the WD is on the verge of collapse rather than explosion for this value: Nomoto & Kondo (1991); YL), $g = 1$ (which is an absolute upper bound: see § 2), $\alpha = 1.7$ (which is the upper end of the semi-empirical range for α that we derived § 5 and is larger than the largest α value of Höflich & Khokhlov (1996) (see § 2)), and $h = 0$ (which is extreme for normal SNe Ia given that spectra until after B -maximum are dominated by IME lines and for SN 2003fg given its early-post- B -maximum spectrum is fairly normal, and so dominated by IME lines).

Given two values of each of $\rho_{\text{central,WD}}$ (i.e., $2.9 \times 10^9 \text{ g cm}^{-3}$ and $10^{10} \text{ g cm}^{-3}$), g (i.e., 0.7 and 1), α (i.e., 1.2 and 1.7), and h (i.e., 1 and 0), there are 16 possibilities which we represent by the 8 SN 2003fg points on the Figures 1 and 2: N ($g = 1, \alpha = 1.7$), O ($g = 1, \alpha = 1.2$), X ($g = 0.7, \alpha = 1.7$), and Y ($g = 0.7, \alpha = 1.2$).

The input parameter values for all the SN 2003fg points and the lower bound masses we derive from them are given in Table 1. Table 1 also gives other output parameter values for the input parameter value sets: i.e., f_{CO} , f_{IME} , f_{IPE} , $f_{^{56}\text{Ni}}$ (which is the mass fraction of ^{56}Ni), v_e , and E . The lower bound masses are actually obtained by solving SSC model using $M_{\text{IPE-core}}$, $v_{\text{IPE-core}}$, $\rho_{\text{central,WD}}$, and h as 4 independent parameters and the procedure given in Appendix C. The last-line parameter values with $v_{\text{IPE-core}} = 8000 \text{ km s}^{-1}$ give no solution for the mass since even a non-rotating WD for the given input parameters is too massive to yield this $v_{\text{IPE-core}}$ value. So we set $v_{\text{IPE-core}} = 7639.5 \text{ km s}^{-1}$ which is the largest $v_{\text{IPE-core}}$ for which a solution exists given the other input parameter values. The output mass is just the mass of a non-rotating WD. The output masses of Table 1 can also be obtained, of course, by interpolation from Figures 1 and 2.

We regard all the output masses in Table 1 as lower bounds on the actual mass since, as

emphasized above, 8000 km s^{-1} is an upper bound on the IPE-core velocity and $7402.947 \text{ km s}^{-1}$ is either an upper bound or at least not far removed from an upper bound.

The lower bound masses in Table 1 are rated by the number of extreme parameter values (EPVs) used to calculate them: the lower the number, the more probable we think the lower bound mass. The most probable set of parameters is for point Y on Figure 1 (0 EPVs) and the least probable is for point N on Figure 2 (4 EPVs) for which in fact there is actually no M solution for $v_{\text{IPE-core}} = 8000 \text{ km s}^{-1}$ as noted above. The least probable set of parameters for a point on Figure 1 are for point N (3 EPVs).

We see that the least probable lower bound masses for each figure (which are those associated with the N points) are approximately the Chandrasekhar mass. Excluding these lower bound masses gives a lowest lower bound mass of $1.62 M_{\odot}$. Excluding lower bound masses with two or more EPVs leaves 5 lower bound masses: the lowest of these is $2.16 M_{\odot}$. The formally most probable lower bound mass (associated with point Y on Fig. 1) according to our rating system is the highest one, $2.84 M_{\odot}$. This lower bound mass is close to the mass estimate of $\sim 3 M_{\odot}$ for SN 2003fg that we obtained from the simple-scaling argument (§ 2).

From the above values we conclude that it is very probable that SN 2003fg is super-Chandrasekhar. The only lower bound masses that are approximately the Chandrasekhar mass are for extreme and improbable sets of the parameters. The more probable sets give lower bound masses that are super-Chandrasekhar and the 5 most probable sets give lower bound masses that are $\gtrsim 2 M_{\odot}$. Given that YL’s binding energy formula is only verified for M in the range $\sim 1.4\text{--}2.05 M_{\odot}$, a SN 2003fg mass $\gtrsim 2 M_{\odot}$ is as much as one can say based on YL’s binding energy formula for rotating super-Chandrasekhar-mass WDs (Appendix B) and the SSC model (§ 4). Given that the analysis of Langer et al. (2000) of accretion histories of WDs in binary systems limits rotating WD mass to $\lesssim 2 M_{\odot}$, our analysis leads to the final conclusion that the mass of SN 2003fg is probably $\sim 2 M_{\odot}$.

The limitation on mass from Langer et al. (2000), has implications for the possible parameter values for g and α . In order to have the SN 2003fg mass $\sim 2 M_{\odot}$, the product of $g\alpha$ would have to be more than the fiducial value of $0.7 \times 1.2 = 0.84$. Demanding $M = 2 M_{\odot}$, solving for $M_{\text{IPE-core}}$ for this M using the $v_{\text{IPE-core}} = 8000 \text{ km s}^{-1}$ and the $\rho_{\text{central,WD}}$ and h values of this section and Newton-Raphson method procedure of Appendix D, and using H2006’s value for $L_{\text{bol}}/\dot{E}_{56\text{Ni}}(t_{\text{bol}})$ of $1.55 M_{\odot}$ allows us to determine $g\alpha$ from

$$g\alpha = \frac{L_{\text{bol}}}{M_{\text{IPE-core}} \dot{E}_{56\text{Ni}}(t_{\text{bol}})} \quad (24)$$

which we obtain using equation (6) of § 2. The $g\alpha$ values we obtain are 1.33 ($\rho_{\text{central,WD}} = 2.9 \times 10^9 \text{ g cm}^{-3}$, $h = 1$), 1.07 ($\rho_{\text{central,WD}} = 2.9 \times 10^9 \text{ g cm}^{-3}$, $h = 0$), 1.21 ($\rho_{\text{central,WD}} =$

$10^{10} \text{ g cm}^{-3}$, $h = 1$), and 1.00 ($\rho_{\text{central,WD}} = 10^{10} \text{ g cm}^{-3}$, $h = 0$). If we also demand that $g = 0.7$ (which as we argued in § 2 seems a good representative fiducial value), then the following α values are needed 1.91 ($\rho_{\text{central,WD}} = 2.9 \times 10^9 \text{ g cm}^{-3}$, $h = 1$), 1.53 ($\rho_{\text{central,WD}} = 2.9 \times 10^9 \text{ g cm}^{-3}$, $h = 0$), 1.72 ($\rho_{\text{central,WD}} = 10^{10} \text{ g cm}^{-3}$, $h = 1$), and 1.44 ($\rho_{\text{central,WD}} = 10^{10} \text{ g cm}^{-3}$, $h = 0$). Since α is really not a well constrained parameter, these α values are not implausible. Only one is significantly outside of the semi-empirical α range of ~ 0.6 – 1.7 we found in § 5. Recall that range is not definitive. Three of the α values are outside of the α range of 0.62–1.46 suggested by the SN Ia models of Höflich & Khokhlov (1996). Recall that range was only suggestive. One must remember that SN 2003fg is a very peculiar and a unique SN Ia, and so its α value is not well constrained by the possible α values of existing SN Ia models and other known SNe Ia.

One last fine point to discuss is related to the gamma-ray-escape effect discussed in § 2. It follows from the discussion in § 2, that the gamma-ray-escape effect should give a tendency to lower α as $f_{56\text{Ni}}$ increases if that increase brings ^{56}Ni matter closer to the surface as, in fact, it does in the SSC model. From Table 1, we see that the parameter sets with $\alpha = 1.2$ have larger $f_{56\text{Ni}}$ values than the counterpart sets with $\alpha = 1.7$ in all cases. Thus, coincidentally (since we are not invoking gamma-rays at all in the SSC model) α varies with $f_{56\text{Ni}}$ in a way that is qualitatively consistent with tendency of the gamma-ray-escape effect.

7. CONCLUSIONS AND DISCUSSION

Our analysis of the data for SN 2003fg supports the conclusion of H2006 that this SN Ia is super-Chandrasekhar (§ 6). We find it very improbable, although not absolutely ruled out, that SN 2003fg has only about a Chandrasekhar mass (the physical Chandrasekhar mass being $1.38 M_{\odot}$ Appendix A) and probable that its mass is $\sim 2 M_{\odot}$ as H2006 also concluded. Our conclusion relies on the adequacy of YL’s binding energy formula for rotating super-Chandrasekhar-mass WDs (Appendix A), the analysis of Langer et al. (2000) that limits WD mass in possible accretion histories to $\lesssim 2 M_{\odot}$, and our SSC model of SN Ia ejecta (§ 4). It is likely that improvements to YL’s binding energy formula will not change our SSC model results qualitatively, unless rotating WDs with masses significantly greater than the Chandrasekhar mass are ruled out by improvements in the input physics of YL’s theory of differential rotation in mass-accreting WDs.

An ultimate verification that SN 2003fg is super-Chandrasekhar would require that only realistic explosion models of super-Chandrasekhar-mass WDs allow a radiative transfer history (calculated with detailed radiative transfer) consistent with observations. Since we do not yet have completely adequate explosion models for any SN Ia, it will probably be

some time before this ultimate verification is possible.

What is the significance of SN 2003fg? Given that as of 2006 September 28 there are 1347 SNe Ia or possible SNe Ia that have been observed according to the Central Bureau for Astronomical Telegrams (2006) (with, of course, a wide range of observational coverage from almost nothing to extensive) and SN 2003fg is the first SN Ia discovered for which there is significant evidence of a significant super-Chandrasekhar mass, we conclude that SN 2003fg-like SNe Ia must be rather rare. Thus, for cosmological evolution and for cosmological distance determinations, SN 2003fg-like SNe Ia are probably of small direct importance.

But for the study of SNe Ia, SN 2003fg may be quite important. As YL point out, it is somewhat surprising that super-Chandrasekhar SNe Ia have not been much considered given that WDs rotate, and thus can be super-Chandrasekhar especially if their rotation is accelerated by accretion. Of course, the lack of observational need to consider super-Chandrasekhar SNe Ia has been a main factor in the relative neglect of such events. Also the relative homogeneity of SNe Ia pointed to a relative of homogeneity progenitors which pointed to maybe only near-Chandrasekhar mass SNe Ia. However, it could be (as YL have discussed at greater length) that there is a distribution of SN Ia progenitor masses from slightly below the Chandrasekhar mass to significantly above it and that the distribution of masses may explain part of the dispersion of SN Ia behavior. This hypothetical distribution is probably fast declining with mass coordinate in the vicinity of the probable mass of SN 2003fg given that SN 2003fg-like SNe Ia seem so rare. In fact, it is possible that having a small super-Chandrasekhar mass is an important ingredient in normal SNe Ia explosions and radiative transfer histories. This is a speculation, but one that is hard to ignore in light of SN 2003fg.

Support for this work has been provided by NASA grant NAG5-3505, NSF grant AST-0506028, and the Homer L. Dodge Department of Physics & Astronomy of the University of Oklahoma. We thank S.-C. Yoon for answers to questions about his work.

A. THE CHANDRASEKHAR MASS

The expression Chandrasekhar mass is used to mean the upper limit on the mass of a non-rotating WD. Above this upper limit, collapse occurs to a neutron star caused by the inability of the pressure of the matter's equation of state (EOS) to sustain the WD against its self-gravity. But what exactly the Chandrasekhar mass is depends on the degree of physical realism specified.

Chandrasekhar in his book on stellar structure (Chandrasekhar 1957, p. 412ff) derives the upper limit based on Newtonian gravity and the zero-temperature, perfect Fermi electron gas in the extreme (special) relativistic limit where the EOS is

$$P = K\rho^{4/3} , \quad (\text{A1})$$

where P is pressure, K is a constant depending on fundamental constants and the composition of the WD, and ρ is (mass) density. It is the electron gas pressure that supports the WD against self-gravity. The WD with this EOS is an index-3 polytrope with a fixed density profile: polytropes being hydrostatic spheres with EOSs of the form

$$P = K\rho^{(n+1)/n} , \quad (\text{A2})$$

where K is a constant and n is the polytropic index (e.g., Chandrasekhar 1957, p. 84ff; Clayton 1983, p. 155ff). From Chandrasekhar’s derivation (also given by, e.g., Shapiro & Teukolsky (1983, p. 61–64)) with the CODATA 2002 fundamental constant values (e.g., NIST 2006) and the modern solar mass value $M_\odot = 1.9891 \times 10^{33}$ g (e.g., Cox 2000, p. 12), one obtains for the mass limit what can be called the formal Chandrasekhar mass,

$$M_{\text{ch,formal}} = \frac{5.8233}{\mu_e^2} M_\odot = 1.4558 \left(\frac{2}{\mu_e} \right)^2 M_\odot , \quad (\text{A3})$$

where the limitation to five significant digits for the coefficients is set by the number of significant digits given for the modern value of the gravitational constant ($G = 6.6742(10) \times 10^{-8}$ in CGS units) and for the modern value of the solar mass. (We used double precision arithmetic to calculate the coefficients for equation (A3) and for all the calculations in this appendix.) The Chandrasekhar mass is independent of density. Thus, we can imagine scaling up the density throughout the WD by a constant factor and make the electron gas more and more relativistic throughout the WD, and thus make the extreme relativistic condition of derivation more and more exact. Thus, Chandrasekhar mass is asymptotically exact for zero-temperature, perfect Fermi electron gas as the density is scaled up toward infinity. The radius of the WD goes asymptotically to zero as $\rho_{\text{central,WD}} \rightarrow \infty$ (e.g., Shapiro & Teukolsky 1983, p. 63). Thus, if mass accretion increases a WD mass toward the Chandrasekhar mass, the WD in the original derivation picture is compacting toward a point mass. At some point in the accretion, one would expect the input physics to break down and some process would prevent compaction to a point mass.

The μ_e quantity in equation (A3) is the mean molecular mass per electron and is given by

$$\frac{1}{\mu_e} = \sum_i \frac{X_i Z_i}{A_i} , \quad (\text{A4})$$

where the sum is over all elements i in the composition, X_i is the mass fraction of element i , Z_i is the atomic number of element i (we assume that the atoms are all completely ionized and the electrons all behave as free particles), and A_i is the atomic mass of element i in atomic mass units (AMUs) (e.g., Clayton 1983, p. 84). The effect of composition on the Chandrasekhar mass enters only through μ_e . For compositions not containing hydrogen or heavy elements $Z_i/A_i \sim 1/2$, and so the fiducial value of μ_e is 2. For a CO WD with equal parts carbon and oxygen and standard atomic masses (which are some kind of terrestrial weighted averages of isotopic atomic masses) (e.g., NIST 2005), $\mu_e = 2.00085$ and $M_{\text{ch}} = 1.4546 M_{\odot}$.

In evaluating the formal Chandrasekhar mass, Chandrasekhar used older fundamental constant values and an older solar mass value, of course. He also used the proton mass where a modern person would probably use the AMU in his formulae, and this required that his atomic masses for evaluating μ_e are in units of the proton mass rather than in units of the AMU (Chandrasekhar 1957, p. 415–416, 432–433). For the first coefficient for equation (A3), Chandrasekhar obtained 5.75 (Chandrasekhar 1957, p. 423) from which the second coefficient value 1.44 follows. The coefficient values 5.75 and 1.44 appear in various places in the literature (e.g., Ostriker & Bodenheimer 1968). Using the fundamental constant values and solar mass value ostensibly used by Chandrasekhar (1957, p. 487) and Chandrasekhar’s definition of μ_e , we obtain for the coefficients 5.7513 and 1.4378 where we quote more digits than are physically significant to allow consistency checks: Chandrasekhar correctly rounded off to 3 digits given the precision of the values he used. If one does the calculations for the coefficients using the EOS parameter values calculated by Chandrasekhar (1957, p. 416) and his gravitational constant ($G = 6.67 \times 10^{-8}$ in CGS units: Chandrasekhar 1957, p. 487) rather than using the older fundamental constant values (except for the gravitational constant) directly (which implies using Chandrasekhar’s definition of μ_e) and using the modern solar mass value, one obtains for the coefficients 5.7444 and 1.4361 where we quote more digits than are physically significant to allow consistency checks. If we used the modern fundamental constant values and solar mass value and Chandrasekhar’s definition of μ_e , the coefficients in equation (A3) would be 5.7395 and 1.4349 to the correct number of significant digits. We report the numbers in this paragraph to illustrate some of the sources of small inconsistencies in formal Chandrasekhar mass values that may appear in the literature.

The formal Chandrasekhar mass is an idealization in several respects. If one makes a correction for general relativity, then there is a collapse caused by gravity that occurs at a finite density which when considered apart from other effects is $2.646 \times 10^{10} (\mu_e/2)^2 \text{ g cm}^{-3}$ (e.g., Shapiro & Teukolsky 1983, p.160) and at mass slightly different from that of equation (A3). Since the collapse occurs at a finite density, the electron gas is not in the extreme relativistic limit throughout the WD and gives rise to another correction for the collapse

mass. The two effects reduce the mass of collapse from $M_{\text{ch,formal}}$ to $1.418 (2/\mu_e)^2 M_\odot$ (e.g., Woosley & Weaver 1994, p. 84). There is also a Coulomb correction to account for the concentration of positive charge into nuclei rather spread uniformly in the electron gas (e.g., Shapiro & Teukolsky 1983, p. 29ff). Adding this effect gives a corrected Chandrasekhar mass M_{ch} :

$$\begin{aligned} M_{\text{ch}} &\approx 1.418 \left(\frac{2}{\mu_e}\right)^2 \left[1 - \frac{3}{5} \left(\frac{12}{\pi}\right)^{1/3} \alpha_{\text{fs}} \langle Z \rangle^{2/3} \right] M_\odot \\ &\approx 1.418 \left(\frac{2}{\mu_e}\right)^2 \left[1 - 0.02259927661 \times \left(\frac{\langle Z \rangle}{6}\right)^{2/3} \right] M_\odot \end{aligned} \quad (\text{A5})$$

(Shapiro & Teukolsky 1983, p. 32; Baron & Cooperstein 1990; Woosley & Weaver 1994, p. 84), where $\alpha_{\text{fs}} = 1/137.03599911(46)$ is the fine structure constant (e.g., NIST 2006) and where we have approximately generalized the expression from the references by replacing atomic number Z by mean atomic number $\langle Z \rangle$. For a CO WD with equal parts carbon and oxygen, $\mu_e = 2.00085$ again, and $\langle Z \rangle = 7$, one obtains $M_{\text{ch}} = 1.38 M_\odot$.

Further corrections to the corrected Chandrasekhar mass are needed for finite temperature (Baron & Cooperstein 1990; Woosley & Weaver 1994, p. 85–86). These corrections increase the corrected Chandrasekhar mass, but for CO WDs they do so by only of order 0.1 %.

In fact, it is believed that non-rotating CO WDs can never reach the exact corrected Chandrasekhar mass (whatever that exactly is) for a density-insensitive EOS. It is believed that WDs can only grow close to the corrected Chandrasekhar mass by accretion. During this process when central density $\rho_{\text{central,WD}}$ reaches of order $10^{10} \text{ g cm}^{-3}$, electron capture on nuclei to make neutrons is likely to induce collapse to a neutron star by rapidly diminishing the electron gas pressure (Nomoto & Kondo 1991; YL). This collapse event depends on the central temperature being low enough, but that seems likely in likely accretion histories. If the central temperature is relatively high (of order $2.5 \times 10^8 \text{ K}$), then unstable carbon burning is likely to lead to thermonuclear explosion when the central density is of order $3 \times 10^9 \text{ g cm}^{-3}$ (e.g., Woosley & Weaver 1994, p. 108). The central density and temperature for collapse or explosion actually do depend on the accretion history and are also are subject to revision with improved input physics. However, at present the non-rotating WD mass at the time of explosive carbon ignition is found to be about $1.38 M_\odot$ (e.g., Woosley & Weaver 1994, p. 108; Nomoto et al. 1984): i.e., close to the zero-temperature corrected Chandrasekhar mass M_{ch} . In the main text, we will just refer to $1.38 M_\odot$ as the Chandrasekhar mass or physical Chandrasekhar mass for brevity.

As a necessary simplification for their rotating WD modeling, YL adopted the zero-

temperature, perfect Fermi electron gas EOS derived by Chandrasekhar in 1935 (Chandrasekhar 1935). This EOS is sometimes called the Chandrasekhar EOS (e.g., Ostriker & Bodenheimer 1968). The Chandrasekhar EOS is more advanced than that used to derive the formal Chandrasekhar mass in that it allows for the full range of special relativistic effects from none to extreme. YL actually use the parameter values for the Chandrasekhar EOS that are given Chandrasekhar’s book (Chandrasekhar 1957, p. 416) and adopt $\mu_e = 2$ for all calculations. By implication, YL should be using Chandrasekhar’s definition of μ_e . With this definition, μ_e should be 1.98640 for equal amounts of carbon and oxygen (calculated using standard atomic masses times the AMU divided by the proton mass), not 2. YL’s value for the Chandrasekhar mass for their non-rotating model with infinite central density is $1.436 M_\odot$ which is just the Chandrasekhar mass value one would calculate using Chandrasekhar’s EOS parameter values, Chandrasekhar’s value of the gravitational constant, the modern solar mass value, Chandrasekhar’s definition of μ_e , and $\mu_e = 2$. YL’s Chandrasekhar mass value was, in fact, determined as just described (Yoon 2006).

Because YL have omitted the general relativistic, Coulomb, and temperature corrections discussed above to the EOS, their masses will likely be in error by a few percent for the given input parameters. The Coulomb correction is probably the most important omission. It tends to reduce mass for a given central density. Thus, YL’s masses are probably overestimates for their specified central densities. Actually, YL’s treatment of the EOS (using older parameter values for the EOS and $\mu_e = 2$ as described just above) may partially compensate for omitting the Coulomb correction. For example, the Coulomb correction reduces the Chandrasekhar mass by about 2.5 % and YL’s treatment reduces the formal Chandrasekhar mass for equal amounts of carbon and oxygen from $1.4546 M_\odot$ (see above) to $1.436 M_\odot$ or by about 1.3 %.

B. THE YOON & LANGER BINDING ENERGY FORMULAE FOR ROTATING SUPER-CHANDRASEKHAR CO WHITE DWARFS AND SOME RELATED RESULTS

The YL formula for the binding energy of rotating super-Chandrasekhar CO WDs is

$$E_{\text{bind}}(\rho_{\text{central,WD}}, M) = E_{\text{bind,NR}}(\rho_{\text{central,WD}}) + E_{\text{bind,coef}}(\rho_{\text{central,WD}}) [M - M_{\text{NR}}(\rho_{\text{central,WD}})]^{1.03} \quad (\text{B1})$$

(YL’s eq. (32)), where the energy units are foe (i.e., units of 10^{51} ergs), $\rho_{\text{central,WD}}$ is the WD central density in grams per centimeter cubed, M is the WD mass in solar mass units,

$$E_{\text{bind,NR}}(\rho_{\text{central,WD}}) = 0.1 \times \left\{ -32.759747 + 6.7179802 \times \log(\rho_{\text{central,WD}}) \right.$$

$$-0.28717609 \times [\log(\rho_{\text{central,WD}})]^2 \} \quad (\text{B2})$$

is the binding energy in foes for a non-rotating WD with central density $\rho_{\text{central,WD}}$ (YL’s eq. (34)),

$$E_{\text{bind,coef}}(\rho_{\text{central,WD}}) = 0.1 \times \left\{ \begin{aligned} & -370.73052 + 132.97204 \times \log(\rho_{\text{central,WD}}) \\ & -16.117031 \times [\log(\rho_{\text{central,WD}})]^2 \\ & +0.66986678 \times [\log(\rho_{\text{central,WD}})]^3 \end{aligned} \right\} \quad (\text{B3})$$

in foes (YL’s eq. (33)), and

$$M_{\text{NR}}(\rho_{\text{central,WD}}) = 1.436 \times \left[1 - \exp \left\{ \begin{aligned} & -0.01316 \times [\log(\rho_{\text{central,WD}})]^{2.706} \\ & +0.2493 \times \log(\rho_{\text{central,WD}}) \end{aligned} \right\} \right] \quad (\text{B4})$$

is the mass in solar mass units of a non-rotating CO WD with central density $\rho_{\text{central,WD}}$ (YL’s eq. (22)). The binding energy formula is a fit to the numerical results of YL and is verified for central densities in the range 10^8 – 10^{10} g cm^{−3} and mass in the range ~ 1.16 – $2.1 M_{\odot}$. Recall from § 2 that the CO WD central density range for explosion as SNe Ia is $\sim 2.5 \times 10^9$ – 10^{10} g cm^{−3} (Woosley et al. 2006; Nomoto & Kondo 1991; YL). We have extrapolated the use of the binding energy formula up to $3 M_{\odot}$.

The formula for $M_{\text{NR}}(\rho_{\text{central,WD}})$ is verified for $\rho_{\text{central,WD}} > 10^7$ g cm^{−3}: for $\rho_{\text{central,WD}} = 2.5 \times 10^9$ g cm^{−3}, it gives $1.384 M_{\odot}$ and for $\rho_{\text{central,WD}} = 10^{10}$ g cm^{−3}, $1.414 M_{\odot}$. Note that as $\rho_{\text{central,WD}}$ goes to infinity, $M_{\text{NR}}(\rho_{\text{central,WD}})$ goes to $1.436 M_{\odot}$. The value $1.436 M_{\odot}$ is the formal Chandrasekhar mass for YL’s choice of equation of state and its parameters (see Appendix A). For the purposes of the investigations of this paper, the differences between $1.436 M_{\odot}$ and the physical Chandrasekhar mass of $1.38 M_{\odot}$ (see Appendix A) and between YL’s equation of state and the exact equation of state are small.

The binding energy formula is, in fact, almost linear in M for a fixed $\rho_{\text{central,WD}}$ (see YL’s Fig. 9). Doing least-squares fits of the binding energy formula to a line for the mass range ~ 1.4 – $3 M_{\odot}$ for the limiting central densities for SNe Ia give

$$E_{\text{bind}}(\rho_{\text{central,WD}} = 2.5 \times 10^9 \text{ g cm}^{-3}, M) = (-1.133 \pm 0.008) + (1.169 \pm 0.003) \times M \quad (\text{B5})$$

and

$$E_{\text{bind}}(\rho_{\text{central,WD}} = 10^{10} \text{ g cm}^{-3}, M) = (-1.923 \pm 0.011) + (1.746 \pm 0.005) \times M, \quad (\text{B6})$$

where again the energy is in foes and the mass in solar mass units. For exploring the behavior of the formula for kinetic energy of a SNe Ia (eq. (18) in § 4), it is, in fact, convenient to use a linear fit to the binding energy. With such a fit, the kinetic energy formula is

$$E \approx E_{\text{IPE}}M[f_{\text{IPE}} + Rh(1 - f_{\text{IPE}})] - a - bM, \quad (\text{B7})$$

where from the above we know that intercept a and slope b vary with allowed central densities for SNe Ia over -1.133 to -1.923 and 1.169 to 1.746 , respectively.

One use of the linear approximation to the binding energy formula is to verify that $\sqrt{2E/M}$ is roughly constant for fixed fractions of explosion-synthesized elements. We made use of this constancy in § 2 in our simple scaling argument for SN Ia mass. Substituting in $E_{\text{IPE}} = 1.61 \text{ foe}/M_{\odot}$ and $R = 0.768$ (see § 2) into equation (B7) and dividing that equation by M gives

$$\frac{E}{M} \approx 1.61 \times [f_{\text{IPE}} + 0.768 \times h(1 - f_{\text{IPE}})] - b + \frac{|a|}{M}. \quad (\text{B8})$$

To have any kind of explosion at all $E/M > 0$, and so the constant term of equation (B8) must be $\gtrsim -|a_{\text{min}}|/M_{\text{ch}} \approx -1.9/1.4 \approx -1.4$ (where $a_{\text{min}} = -1.923$ is the minimum value of a for the $\rho_{\text{central,WD}}$ allowed range). If we choose $f_{\text{IPE}} = 0.648$, $h = 0.798$, and $\rho_{\text{central,WD}} = 2.6 \times 10^9 \text{ g cm}^{-3}$ (which are the values of model W7 (Nomoto et al. 1984; Thielemann et al. 1986)) as representative of SN Ia explosions, then $a = -1.15$ and $b = 1.18$ (from a least-squares fit to the binding energy formula over the mass range $\sim 1.4\text{--}3 M_{\odot}$ with $\rho_{\text{central,WD}} = 2.6 \times 10^9 \text{ g cm}^{-3}$) and the first term of equation (B8) is 1.39. (Note $f_{\text{IPE}} = 0.648$ and $h = 0.798$, imply $f_{\text{CO}} = 0.0711$ and $f_{\text{IME}} = 0.281$ using equation (17) in § 4.) Substituting the calculated values for a , b , and the first term of equation (B8) into equation (B8) gives

$$\frac{E}{M} \approx 0.21 + \frac{1.15}{M}. \quad (\text{B9})$$

Thus, with the representative values, an explosion can be expected for any M since the constant term of equation (B9) is positive, but the value of E/M can only be very crudely approximated as a constant with respect to M . However, $\sqrt{2E/M}$ will be closer to constancy and we can accept that it is so crudely. (Making use of equation (B9) and converting units, we find for M going from $1.38 M_{\odot}$ to $3 M_{\odot}$ that $\sqrt{2E/M}$ goes from 10260 km s^{-1} to 7750 km s^{-1} .) This constancy verifies one of our assumptions for the simple scaling argument provided that the SSC model is valid up to $\sim 3 M_{\odot}$ which requires that the usage of YL’s binding energy formula can be extrapolated to $3 M_{\odot}$.

C. SOLVING THE SSC MODEL FOR MASS TREATED AS A DEPENDENT PARAMETER

To calculate Figures 1 and 2, we used the SSC model mass M as an independent parameter. (See §§ 2 and 4 for a description of the parameters and the SSC model.) One can make M a dependent parameter and replace it among the independent parameters with $v_{\text{IPE-core}}$. The solution for M can then be done via the Newton-Raphson method (e.g., Press et al. 1992, p. 355ff) with IPE-core mass $M_{\text{IPE-core}}$, IPE-core velocity $v_{\text{IPE-core}}$ (now independent), central density $\rho_{\text{central,WD}}$, and h as the 4 independent parameter values. We assume the independent parameter values are given. The dependent parameters besides M are the e -folding velocity v_e , kinetic energy E , and the mass fractions f_{CO} , f_{IME} , and f_{IPE} .

The Newton-Raphson method starts with an initial input mass M_1 (for which we suggest an initial value below) and iterates to improve the input values toward the true value for M . The steps of the iteration are as follows. An input M_i for the i th iteration along with the given $M_{\text{IPE-core}}$, $\rho_{\text{central,WD}}$ and h values are used to evaluate the following version of the kinetic energy formula (see eq. (18) in § 4):

$$E = E_{\text{IPE}}[M_{\text{IPE-core}} + Rh(M - M_{\text{IPE-core}})] - E_{\text{bind}}(\rho_{\text{central,WD}}, M) , \quad (\text{C1})$$

where we have used the fact that $M_{\text{IPE-core}} = M f_{\text{IPE}}$ (see eq. (4) in § 2) to eliminate f_{IPE} from equation (18). Using the calculated i th iteration kinetic energy E_i , we obtain the i th iteration e -folding velocity

$$v_{e,i} = \sqrt{\frac{B E_i}{6 M_i}} , \quad (\text{C2})$$

where we have used equation (12) (§ 4), but with assumption that E_i is in foe and M_i is in solar mass units, and so need conversion factor $B = 10^{51}$ ergs foe $^{-1}/M_{\odot}$ to give $v_{e,i}$ in CGS units. The i th iteration IPE-core reduced velocity $x_{\text{IPE-core},i} = v_{\text{IPE-core}}/v_{e,i}$ (see eq. (14) in § 4) (assuming the given $v_{\text{IPE-core}}$ value is in CGS units). One then uses equation (15) (§ 4), to find the i th iteration $f_{\text{IPE},i}$ and then the i th iteration output mass $M_{\text{out},i}$ of the iteration follows from

$$M_{\text{out},i} = \frac{M_{\text{IPE-core}}}{f_{\text{IPE},i}} , \quad (\text{C3})$$

where we have made use of equation (4) in (§ 2) For the Newton-Raphson method iteration, the quantity whose zero we want to find as a function of M is $M_{\text{out}} - M$. The i th iteration Newton-Raphson correction ΔM_i to approximately zero $M_{\text{out}} - M$ is given by

$$\Delta M_i = - \left(\frac{M_{\text{out}} - M}{dM_{\text{out}}/dM - 1} \right) \Big|_{M_i} . \quad (\text{C4})$$

It is straightforward to show that the i th iteration value of the derivative dM_{out}/dM is given by

$$\begin{aligned} \left. \frac{dM_{\text{out}}}{dM} \right|_{M_i} &= - \left(\frac{M_{\text{IPE-core}}}{f^2} \frac{df}{dx} \frac{dx}{dv_e} \frac{dv_e}{dw} \frac{dw}{dM} \right) \Big|_{M_i} \\ &= \left(\frac{M_{\text{IPE-core}}}{f_{\text{IPE},i}^2} \right) \left[\frac{x_{\text{IPE-core},i}^3 \exp(-x_{\text{IPE-core},i})}{24} \right] \left(\frac{B}{v_{e,i}^2} \right) \left[\frac{d(E/M)}{dM} \right] \Big|_{M_i}, \end{aligned} \quad (\text{C5})$$

where $w = (B/6)(E/M)$,

$$\frac{d(E/M)}{dM} = \frac{E_{\text{IPE}}Rh - dE_{\text{bind}}/dM}{M} - \frac{E}{M^2}, \quad (\text{C6})$$

and

$$\frac{dE_{\text{bind}}}{dM} = 1.03 \times E_{\text{bind,coef}}(\rho_{\text{central,WD}}) [M - M_{\text{NR}}(\rho_{\text{central,WD}})]^{0.03}. \quad (\text{C7})$$

The last equation was obtained by differentiation from equation (B1).

The Newton-Raphson method in this case converges quite quickly in practice. The guarantee of convergence is that $M_{\text{out}} - M$ is strictly decreasing with respect to M with no stationary points for the allowed $\rho_{\text{central,WD}}$ range for SN Ia explosion of $\sim 2.5 \times 10^9 - 10^{10} \text{ g cm}^{-3}$ (Woosley et al. 2006; Nomoto & Kondo 1991; YL). This means that the Newton-Raphson correction ΔM_i always has the correct sign and if the corrections are prevented from causing any overshooting of the diminishing allowed range for the true mass M , then convergence must follow. All that is required to show the strictly decreasing nature of $M_{\text{out}} - M$ is to show that E/M is monotonically decreasing with respect to M with a stationary point only at $M = \infty$. This is clear from equation (C5) since all the factors on the right-hand side of the second expression are clearly always positive or zero except for $d(E/M)/dM$. (Note that $M_{\text{out}} - M$ has no stationary points even though $d(E/M)/dM$ and dM_{out}/dM do because the $-M$ term derivative is -1 .)

Because of the unusual exponent in the binding energy formula (see eq. (B1) in Appendix B), it is awkward and not enlightening to work with the exact formula for kinetic energy equation (C1). Instead we will show that E/M is monotonically decreasing with respect to M using the kinetic energy formula with the linear binding energy formula approximation: see equation (B7) in Appendix B. First, we rewrite equation (B7) in terms of the proper variables for the Newton-Raphson method:

$$\begin{aligned} E &\approx E_{\text{IPE}}[M_{\text{IPE-core}} + Rh(M - M_{\text{IPE-core}})] - a - bM \\ &= E_{\text{IPE}}M_{\text{IPE-core}}(1 - Rh) - a + (E_{\text{IPE}}Rh - b)M, \end{aligned} \quad (\text{C8})$$

where we note that the intercept term $E_{\text{IPE}}M_{\text{IPE-core}}(1 - Rh) - a > 0$ always since $1 - Rh > 0$ always and $a < 0$ for all linear fits to the binding energy formula for its allowed $\rho_{\text{central,WD}}$

range (see Appendix B). The sign of the slope $E_{\text{IPE}}Rh - b$ depends on the relative sizes of h and b . Using the model W7 (Nomoto et al. 1984; Thielemann et al. 1986) values $h = 0.798$ and $b = 1.18$, we find that $E_{\text{IPE}}Rh - b = -0.19$: thus, what we can take as the representative slope of equation (C8) is negative. Using equation (C8), we obtain

$$\frac{E}{M} \approx \frac{E_{\text{IPE}}M_{\text{IPE-core}}(1 - Rh) - a}{M} + E_{\text{IPE}}Rh - b, \quad (\text{C9})$$

and then differentiating E/M we get

$$\frac{d(E/M)}{dM} \approx - \left[\frac{E_{\text{IPE}}M_{\text{IPE-core}}(1 - Rh) - a}{M^2} \right]. \quad (\text{C10})$$

Since $E_{\text{IPE}}M_{\text{IPE-core}}(1 - Rh) - a > 0$ always, it is clear within our approximation for E that E/M is monotonically decreasing with the only stationary point at $M = \infty$. Now we have shown this behavior only for the approximate equation (C9). But since this equation is, in fact, a very good approximation to equation (C1) divided by M and the behavior is robust for all allowed values of a (see Appendix B), we conclude that E/M is to at least good accuracy monotonically decreasing with M in general with a stationary point only at $M = \infty$. It then follows from equation (C5) that $M_{\text{out}} - M$ is to at least good accuracy strictly decreasing with M . This is what we needed to show to prove that the Newton-Raphson method would always converge for the allowed $\rho_{\text{central,WD}}$ range.

We can deduce some approximate limiting behaviors of the M_{out} function by making use of equation (C9). If $E_{\text{IPE}}Rh - b \leq 0$ (which we take to be the representative case) and M is increased, then at some point (which is at finite M if $E_{\text{IPE}}Rh - b < 0$ and infinite M otherwise) $E/M \rightarrow 0$, $v_e \rightarrow 0$, $x \rightarrow \infty$, $f \rightarrow 1$, and $M_{\text{out}} \rightarrow M_{\text{IPE-core}}$. On the other hand, if $E_{\text{IPE}}Rh - b > 0$ and $M \rightarrow \infty$, then E/M , v_e , x , f , and M_{out} approach asymptotically to a finite positive value, a finite positive value, a finite positive value, a finite positive value less than 1, and a finite positive value greater than $M_{\text{IPE-core}}$, respectively. If $M \rightarrow 0$, then $E/M \rightarrow \infty$, $v_e \rightarrow \infty$, $x \rightarrow 0$, $f \rightarrow 0$, and $M_{\text{out}} \rightarrow \infty$. Actually, we cannot let $M \rightarrow 0$ in the M_{out} function since YL’s binding energy formula has no solution for $M < M_{\text{NR}}$.

What is the appropriate initial value M_1 for the Newton-Raphson method? Well the lower bound on the true value for M is clearly

$$M_{\text{lower bound}} = \max [M_{\text{IPE-core}}, M_{\text{NR}}(\rho_{\text{central,WD}})] \quad (\text{C11})$$

since a physical M cannot be less than the input core mass $M_{\text{IPE-core}}$ nor than the mass of a non-rotating WD for the input density $M_{\text{NR}}(\rho_{\text{central,WD}})$. In practice, we have found $M_{\text{lower bound}}$ to work well as an initial value M_1 .

If we use $M_{\text{lower bound}}$ as an input mass M and find that $M_{\text{out}}(M_{\text{lower bound}}) < M_{\text{lower bound}}$, then there is no solution since Newton-Raphson correction from equation (C4) will be negative. Recall that Newton-Raphson correction always has the correct sign for our case, and so a negative correction to the lower bound on M implies there is no solution. One way of looking at this case is to say there is not enough nuclear burning energy released with any allowed value of M to match the input $v_{\text{IPE-core}}$. On Figures 1 and 2, the no-solution case with $M_{\text{lower bound}} = M_{\text{NR}}(\rho_{\text{central,WD}})$ and $M_{\text{out}}(M_{\text{lower bound}}) < M_{\text{NR}}(\rho_{\text{central,WD}})$ would correspond to having the point $(M_{\text{IPE-core}}, v_{\text{IPE-core}})$ in the region to the left of the M_{NR} mass curves: if it was to the right, there would be a solution. This no-solution case is actually the case for the point N on Figure 2 for $h = 0$ (which means $f_{\text{IME}} = 0$ recall) (see § 6).

If $M_{\text{lower bound}}$ gives $E < 0$, then there is also no solution mass M . Since the intercept term of equation (C8) is always positive, then $E < 0$ for any input M implies the slope is negative. This means that the approximate kinetic energy function (and the exact kinetic energy function to high accuracy) can only grow more negative for M increasing beyond $M_{\text{lower bound}}$. Thus for no allowed M is the kinetic energy positive which is required for an explosion. There is not enough nuclear burning energy for any allowed M to explode the WD with the input parameter values in this case.

The true values for f_{IPE} , v_e , kinetic energy E , and mass M are obtained from the Newton-Raphson iteration. The true values of f_{CO} and f_{IME} are obtained using the h and f_{IPE} values in equation (17) (§ 4).

Note that if we had used either of f_{CO} or f_{IME} as an independent parameter instead of h , we would have to deal with an extra check on whether or not a given converged solution M was physically allowed. If we used f_{CO} (f_{IME}) as an independent parameter and solved for M and then found that $f_{\text{IME}} < 0$ ($f_{\text{CO}} < 0$), the found solution M would be ruled out: i.e., there would be no physically allowed solution for the given input parameter values. Using h as an independent parameter eliminates this complication for valid h (i.e., h in the range 0–1) and a solution mass $M \geq M_{\text{lower bound}}$, since one will only obtain valid f_{CO} and f_{IME} values from equation (17) (§ 4): i.e., values in the range 0–1. Thus, the solution mass M can be known to be valid without having to check on the f_{CO} or f_{IME} values. The above discussion shows why we prefer using h as an independent parameter to either of f_{CO} or f_{IME} .

D. SOLVING THE SSC MODEL FOR CORE MASS TREATED AS A DEPENDENT PARAMETER

In this appendix, we show how to solve the SSC model for core mass $M_{\text{IPE-core}}$ treated as a dependent parameter. The independent parameters are now mass M , IPE-core velocity $v_{\text{IPE-core}}$, WD central density $\rho_{\text{central,WD}}$, and h . We assume the independent parameter values are given. The dependent parameter besides $M_{\text{IPE-core}}$ are the e -folding velocity v_e , kinetic energy E , and mass fractions f_{CO} , f_{IME} , and f_{IPE} . The solution is by the Newton-Raphson method (e.g., Press et al. 1992, p. 355ff) and is similar to that of Appendix C, but is somewhat simpler since the binding energy formula (eq. (B1 in Appendix B) does not depend on $M_{\text{IPE-core}}$.

The Newton-Raphson method iteration starts with an initial input core mass $M_{\text{IPE-core},1}$ (for which we suggest an initial value below) and iterates to improve the input values toward the true value for $M_{\text{IPE-core}}$. The steps of the iteration are as follows. An input $M_{\text{IPE-core},i}$ for the i th iteration is used to evaluate the i th iteration kinetic energy and e -folding velocity $v_{e,i}$ using, respectively, equations (C1) and (C2). The i th iteration IPE-core reduced velocity $x_{\text{IPE-core},i} = v_{\text{IPE-core}}/v_{e,i}$ (see eq. (14) in § 4) (assuming the given $v_{\text{IPE-core}}$ value is in CGS units). One then uses equation (15) (§ 4), to find the i th iteration $f_{\text{IPE},i}$ and then the i th iteration output core mass $M_{\text{IPE-core,out},i}$ follows from

$$M_{\text{IPE-core,out},i} = M f_{\text{IPE},i} , \quad (\text{D1})$$

where we have used equation (4) (§ 2). For the Newton-Raphson method iteration, the quantity whose zero we want to find as a function of $M_{\text{IPE-core}}$ is $M_{\text{IPE-core,out}} - M_{\text{IPE-core}}$. The i th iteration Newton-Raphson correction $\Delta M_{\text{IPE-core},i}$ to approximately zero $M_{\text{IPE-core,out}} - M_{\text{IPE-core}}$ is given by

$$\Delta M_{\text{IPE-core},i} = - \left(\frac{M_{\text{IPE-core,out}} - M_{\text{IPE-core}}}{dM_{\text{IPE-core,out}}/dM_{\text{IPE-core}} - 1} \right) \Bigg|_{M_{\text{IPE-core},i}} . \quad (\text{D2})$$

It is straightforward to show that the i th iteration derivative $dM_{\text{IPE-core,out}}/dM_{\text{IPE-core}}$ is given by

$$\begin{aligned} \frac{dM_{\text{IPE-core,out}}}{dM_{\text{IPE-core}}} \Bigg|_{M_{\text{IPE-core},i}} &= \left(M \frac{df}{dx} \frac{dx}{dv_e} \frac{dv_e}{dw} \frac{dw}{dM_{\text{IPE-core}}} \right) \Bigg|_{M_{\text{IPE-core},i}} \\ &= - \left[\frac{x_{\text{IPE-core},i}^3 \exp(-x_{\text{IPE-core},i})}{24} \right] \\ &\quad \times \left(\frac{B}{v_{e,i}^2} \right) E_{\text{IPE}} (1 - Rh) , \end{aligned} \quad (\text{D3})$$

where $w = (B/6)(E/M)$. The derivative $dM_{\text{IPE-core,out}}/dM_{\text{IPE-core}} \leq 0$ always with the equality holding only for $x_{\text{IPE-core},i} = 0$ and $x_{\text{IPE-core},i} = \infty$. (Note $x_{\text{IPE-core},i}^3/v_{e,i}^2 = x_{\text{IPE-core},i}^5/v_{\text{IPE-core}}^2$.) Thus, the Newton-Raphson method is guaranteed to converge to the true $M_{\text{IPE-core}}$ value since $M_{\text{IPE-core,out}} - M_{\text{IPE-core}}$ is strictly decreasing with $M_{\text{IPE-core}}$ provided the Newton-Raphson corrections are prevented from causing any overshooting of the diminishing allowed range for the converged solution and provided the independent parameter values allow a valid $M_{\text{IPE-core}}$ solution (i.e., one in the range $0-M$). (Note that $M_{\text{IPE-core,out}} - M_{\text{IPE-core}}$ has no stationary points even though $M_{\text{IPE-core,out}}$ does because the $-M_{\text{IPE-core}}$ term derivative is -1 .)

The true f_{IPE} , e -folding velocity v_e , kinetic energy E , and mass $M_{\text{IPE-core}}$ values are obtained from the iteration. The true values of f_{CO} and f_{IME} are obtained using the h and f_{IPE} values in equation (17) (§ 4).

A good initial input $M_{\text{IPE-core},1}$ for Newton Raphson iteration is $M/2$ which is just the midpoint of the allowed range $0-M$.

REFERENCES

- Arnett, W. D. 1979, ApJ, 230, L37
- Arnett, W. D. 1982, ApJ, 253, 785
- Asplund, M., Grevesse, N., & Sauval, A. J. 2005, in ASP Conf. Ser. 336, Cosmic Abundances as Records of Stellar Evolution and Nucleosynthesis, ed. T. G. Barnes III & F. N. Bash (San Francisco: ASP), 25, astro-ph/0410214
- Baron, E., Bongard, S., Branch, D., & Hauschildt, P. H. 2006, ApJ, 645, 480
- Baron, E., & Cooperstein, J. 1990, ApJ, 353, 597
- Benetti, S., et al. 2005, ApJ, 623, 1011
- Branch, D. 1992, ApJ, 392, 35
- Branch, D., Baron, E., Hall, N., Melakayil, M., & Parrent, J. 2005, PASP, 117, 545
- Branch, D., et al. 2003, AJ, 126, 1489
- Branch, D., et al. 2006, PASP, 118, 560
- Central Bureau for Astronomical Telegrams 2006, (Cambridge, Massachusetts: Center for Astrophysics), <http://cfa-www.harvard.edu/iau/cbat.html>

- Chandrasekhar, S. 1935, MNRAS, 95, 207
- Chandrasekhar, S. 1957, *An Introduction to the Study of Stellar Structure* (New York: Dover Publications, Inc.)
- Clayton, D. D. 1983, *Principles of Stellar Evolution and Nucleosynthesis* (Chicago: The University of Chicago Press)
- Conley, A., et al. 2006, AJ, 132, 1707
- Cox, A. N. (ed.) 2000, *Allen's Astrophysical Quantities*, 4th Edition (New York: AIP/Springer-Verlag)
- Dwarkadas, V. V., & Chevalier, R. A. 1998, ApJ, 497, 807
- Firestone, R. B., & Ekström, L. P. 2004, LBNL Isotopes Project-Lunds Universitet: WWW Table of Radioactive Isotopes (Berkeley, California: Lawrence Berkeley National Laboratory), <http://ie.lbl.gov/toi/>
- Fisher, A., Branch, D., Hatano, K., & Baron, E. 1999, MNRAS, 304, 67
- Gibson, B. K., & Stetson, P. B. 2001, ApJ, 547, L103
- Höflich, P., & Khokhlov, A. 1996, ApJ, 457, 500
- Höflich, P., Wheeler, J. C., & Thielemann, F.-K. 1998, ApJ, 495, 617
- Howell, D. A., Höflich, P., Wang, L., & Wheeler, J. C. 2001, ApJ, 556, 302
- Howell, D. A., et al. 2006, Nature, 443, 308 (H2006)
- Jeffery, D. J. 1999, astro-ph/9907015
- Jeffery, D. J., Leibundgut, B., Kirshner, R. P., Benetti, S., Branch, D., & Sonneborn, G. 1992, ApJ, 397, 304
- Khokhlov, A., Müller, E., & Höflich, P. 1993, A&A, 270, 223
- Kirshner, R. P., et al. 1993, ApJ, 415, 589
- Langer, N., Deutschmann, A., Wellstein, S., & Höflich, P. 2000, A&A, 362, 1046
- Livne, E., & Glasner, A. 1990, ApJ, 361, 244
- Livne, E., & Glasner, A. 1991, ApJ, 370, 272

- Mazzali, P. A., Cappellaro, E., Danziger, I. J., Turatto, M., & Benetti, S. 1998, *ApJ*, 499, L49
- Mazzali, P. A., Chugai, N., Turatto, M., Lucy, L. B., Danziger, I. J., Cappellaro, E., Della Valle, M., & Benetti, S. 1997, *MNRAS*, 284, 151
- NIST (National Institute of Standards and Technology) 2005, *Atomic Weights and Isotopic Compositions with Relative Atomic Masses* (Gaithersberg, Maryland: NIST), <http://physics.nist.gov/PhysRefData/Compositions/index.html>
- NIST (National Institute of Standards and Technology) 2006, *The NIST Reference on Constants, Units, and Uncertainties* (Gaithersberg, Maryland: NIST), <http://physics.nist.gov/cuu/Constants/>
- Nomoto, K., & Kondo, Y. 1991, *ApJ*, 367, L19
- Nomoto, K., Thielemann, F.-K., & Yokoi, K. 1984, *ApJ*, 286, 644
- Nugent, P., Baron, E., Branch, D., Fisher, A., & Hauschildt, P. 1997 *ApJ*, 485, 812
- Ostriker, J. P., & Bodenheimer, P. 1968, *ApJ*, 151, 1089
- Phillips, M. M. 1993, *ApJ*, 413, L105
- Phillips, M. M., Lira, P., Suntzeff, N. B., Schommer, R. A., Hamuy, M., & Maza, J. 1999, *AJ*, 118, 1766
- Piersanti, L., Gagliardi, S., Iben, I., Jr., & Tornambe, A. 2003, *ApJ*, 598, 1229
- Pizzochero, P. 1990, *ApJ*, 354, 333
- Press, W. H., Teukolsky, S. A., Vetterling, W. T., & Flannery, B. P. 1992, *Numerical Recipes in Fortran* (Cambridge: Cambridge University Press), <http://library.lanl.gov/numerical/index.html>
- Richardson, D., Branch, D., Casebeer, D., Millard, J., Thomas, R. C., & Baron, E. 2002, *AJ*, 123, 745
- Ruiz-Lapuente, P., Kirshner, R. P., Phillips, M. M., Challis, P. M., Schmidt, B. P., Filippenko, A. V., & Wheeler, J. C. 1995, *ApJ*, 439, 60
- Saha, A., Sandage, A., Thim, F., Labhardt, L., Tammann, G. A., Christensen, J., Panagia, N., & Macchetto, F. D. 2001, *ApJ*, 551, 973

- Saio, H., & Nomoto, K. 2004, *ApJ*, 615, 444
- Shapiro, S. L., & Teukolsky, S. A. 1983, *Black Holes, White Dwarfs, and Neutron Stars: The Physics of Compact Objects* (New York: John Wiley & Sons)
- Thielemann, F.-K., Nomoto, K., & Yokoi, K. *A&A*, 158, 17
- Wang, L., et al. 2003, *ApJ*, 591, 1110
- Webbink, R. F. 1984, *ApJ*, 277, 355
- Wiese, W. L., Smith, M. W., & Glennon, B. M. 1966, in *NSRDS–NBS 4, Atomic Transition Probabilities: Vol. I—Hydrogen through Neon* (Washington, DC: Government Printing Office)
- Wiese, W. L., Smith, M. W., & Miles, B. M. 1969, in *NSRDS–NBS 22, Atomic Transition Probabilities: Vol. 2—Sodium through Calcium* (Washington, DC: Government Printing Office)
- Woosley, S. E. 1991, in *Gamma-Ray Line Astrophysics*, ed. P. Durouchoux & N. Prantzos (Paris: American Institute of Physics), 270
- Woosley, S. E., Kasen, D., Blinnikov, S., & Sorokina, E. 2006, *ApJ*, submitted, [astro-ph/0609562](https://arxiv.org/abs/astro-ph/0609562)
- Woosley, S. E., & Weaver, T. A. 1994, in *Supernovae: Session LIV of the Les Houches École d’Été de Physique Théorique*, ed. S. A. Bludman, R. Mochkovitch, & J. Zinn-Justin (Amsterdam: North-Holland), 63
- Yoon, S.-C. 2006, private communication
- Yoon, S.-C., & Langer, N. 2005, *A&A*, 435, 985 (YL)

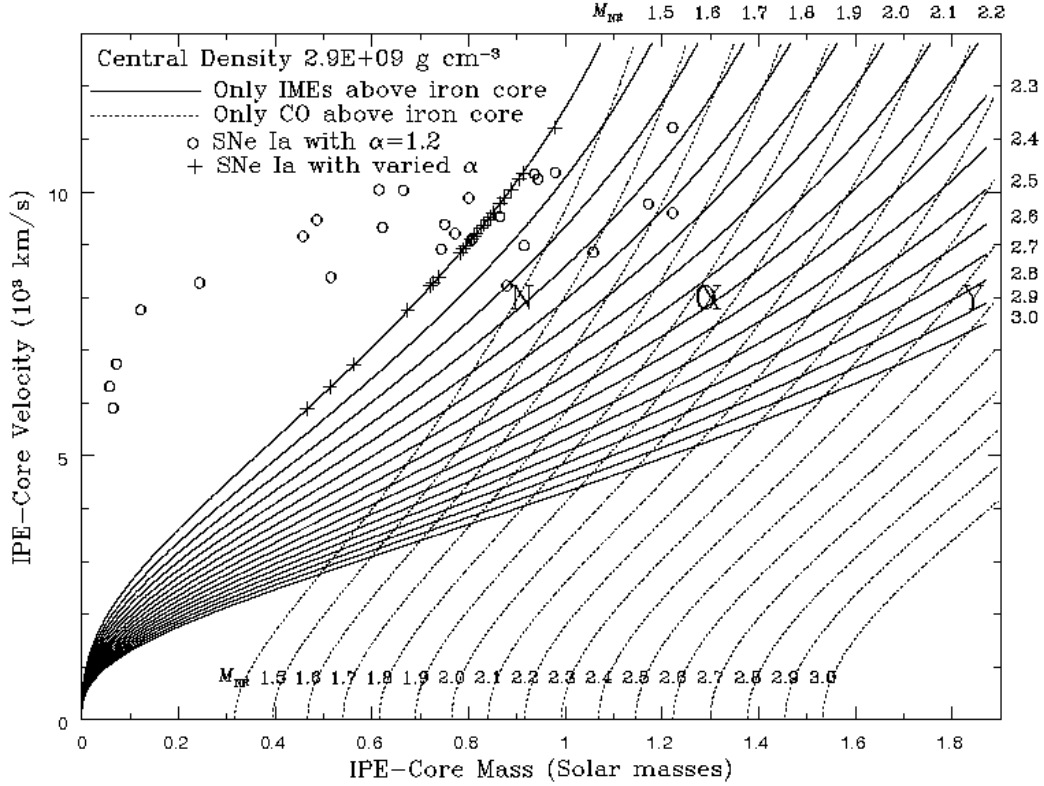


Fig. 1.— Curves of constant SN Ia mass from the SSC model for super-Chandrasekhar-mass SNe Ia on a plot of IPE-core velocity versus IPE-core mass. There are two families of curves: the solid curves are for only IMEs above the IPE core ($h = 1$) and the dotted curves are for only CO above the IPE core ($h = 0$). This plot is calculated for WD progenitors with central density $2.9 \times 10^9 \text{ g cm}^{-3}$. The plot and the data points are explained at length in the text (§§ 4, 5, and 6).

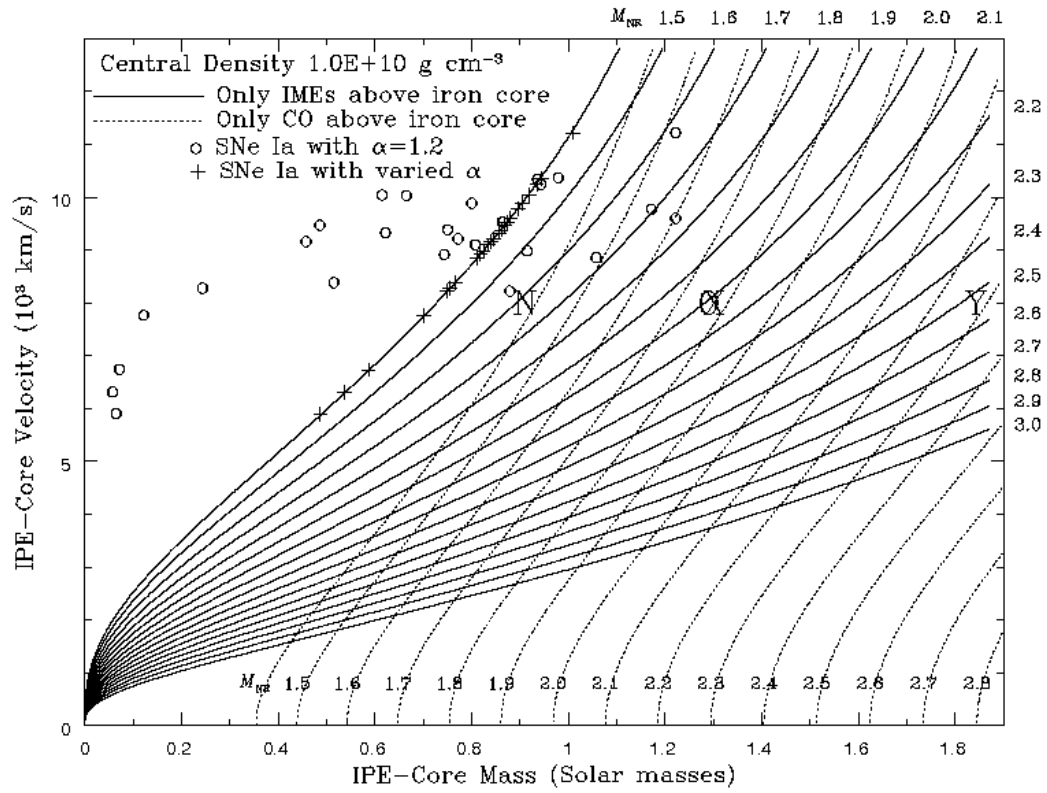


Fig. 2.— The same as Figure 1, except that the plot is calculated for WD progenitors with central density $10^{10} \text{ g cm}^{-3}$.

Table 1. LOWER BOUND MASSES AND OTHER OUTPUT PARAMETERS FOR
SN 2003fg FOR VARIOUS CHOICES OF INPUT PARAMETERS FOR THE SSC
MODEL

Symbol ^a	$M_{\text{IPE-core}}^{\text{b}}$ (M_{\odot})	$\rho_{\text{central,WD}}^{\text{c}}$ (10^9g cm^{-3})	g^{d}	α^{e}	h^{f}	No. of ^g EPVs	M_{LB}^{h} (M_{\odot})	f_{CO}^{i}	$f_{\text{IME}}^{\text{j}}$	$f_{\text{IPE}}^{\text{k}}$	$f_{^{56}\text{Ni}}^{\text{l}}$	v_e^{m} (km s^{-1})	kinetic energy E^{n} (foes)
Y	1.84	2.9	0.7	1.2	1.0	0	2.84	0.000	0.350	0.650	0.455	2390	1.933
Y	1.84	2.9	0.7	1.2	0.0	1	2.44	0.245	0.000	0.755	0.528	2024	1.194
X	1.30	2.9	0.7	1.7	1.0	1	2.17	0.000	0.402	0.598	0.419	2583	1.731
X	1.30	2.9	0.7	1.7	0.0	2	1.84	0.294	0.000	0.706	0.494	2191	1.055
O	1.29	2.9	1.0	1.2	1.0	1	2.16	0.000	0.403	0.597	0.597	2587	1.726
O	1.29	2.9	1.0	1.2	0.0	2	1.83	0.295	0.000	0.705	0.705	2195	1.052
N	0.91	2.9	1.0	1.7	1.0	2	1.68	0.000	0.457	0.543	0.543	2803	1.571
N	0.91	2.9	1.0	1.7	0.0	3	1.40	0.348	0.000	0.652	0.652	2383	0.947
Y	1.84	10.0	0.7	1.2	1.0	1	2.52	0.000	0.269	0.731	0.512	2104	1.332
Y	1.84	10.0	0.7	1.2	0.0	2	2.28	0.191	0.000	0.809	0.566	1840	0.920
X	1.30	10.0	0.7	1.7	1.0	2	2.02	0.000	0.354	0.646	0.452	2406	1.392
X	1.30	10.0	0.7	1.7	0.0	3	1.77	0.266	0.000	0.734	0.514	2095	0.929
O	1.29	10.0	1.0	1.2	1.0	2	2.00	0.000	0.356	0.644	0.644	2414	1.394
O	1.29	10.0	1.0	1.2	0.0	3	1.76	0.268	0.000	0.732	0.732	2102	0.929
N	0.91	10.0	1.0	1.7	1.0	3	1.62	0.000	0.438	0.562	0.562	2726	1.437
N	0.91	10.0	1.0	1.7	0.0	4	1.414 ^o	0.356	0.000	0.644	0.644	2304	0.896

^a Symbol is the symbol used for the data point on Figures 1 and 2.

^b This is the IPE-core mass. It depends inversely on the g and α parameters. In fact $M_{\text{IPE-core}}g\alpha = 1.55 M_{\odot}$. We make the approximation that the IPE core contains all explosion-synthesized IPEs and that no explosion-synthesized IPEs are outside the IPE core.

^c The $\rho_{\text{central,WD}}$ quantity is the central density of the progenitor CO WD.

^d The g factor is the ratio of ^{56}Ni mass to IPE mass which we also take to the IPE-core mass $M_{\text{IPE-core}}$.

^e The α quantity is the bolometric-luminosity-maximum-light ratio of luminosity to the total instantaneous radioactive decay energy release rate per unit ^{56}Ni mass.

^f The $h = f_{\text{IME}}/(f_{\text{CO}} + f_{\text{IME}})$ quantity is the fraction of non-IPE element matter in the ejecta that is explosively-synthesized IME matter.

^g This is the number of extreme parameter values (EPVs) used in determining the lower bound mass.

^h The M_{LB} quantities are the lower bound masses for the given input parameters to the SSC model.

ⁱ The f_{CO} quantity is the mass fraction of CO in the ejecta.

^j The f_{IME} quantity is the mass fraction of IMEs in the ejecta.

^k The f_{IPE} quantity is the mass fraction of IPEs in the ejecta and also interior mass fraction of the IPE core.

^l The $f_{^{56}\text{Ni}}$ quantity is the mass fraction of ^{56}Ni in the ejecta. It equals f_{IPE} when $g = 1$.

^m The v_e quantity is the e -folding velocity of the ejecta.

ⁿ This is the kinetic energy of the ejecta in foes ($1 \text{ foe} = 10^{51} \text{ ergs}$).